SLAC-R-493
UC-414

A MEASUREMENT OF THE ELECTRO WEAK ASYMMETRY PARAMETER FOR THE TAU LEPTON USING THE 1993 AND 1994-95 SLD DATA SAMPLE*

Brett Day Bolen

Stanford Linear Accelerator Center
Stanford University
Stanford, California 94309

SLAC-Report-493
July 1996

Prepared for the Department of Energy
under contract numbers DE-AC03-76SF00515

Printed in the United States of America. Available from the National Technical Information Service, U.S. Department of Commerce, 5285 Port Royal Road, Springfield, Virginia 22161.

*Ph.D. thesis, University of Mississippi.

A Measurement of the Electroweak Asymmetry Parameter for the Tau Lepton using the 1993 and 1994-95 SLD Data Sample

By

Brett Day Bolen

B.S. University of Evansville, 1993

A Thesis
Submitted to the Faculty of
The University of Mississippi
in Partial Fulfillment of the Requirements
for the Degree of Master of Science
in the Department of Physics

The University of Mississippi
July 1996

Dedication

This thesis is dedicated to my parents

Dr. Lee N. Bolen and Mrs. Modine D. Bolen

Thank you for all your help and support

Acknowledgments

First and foremost, I would like to thank my advisor: Dr. Robert Kroeger. It goes without saying that this thesis and the work behind it would not have been done without his help and wisdom. I would also like to thank Dr. James Reidy and Dr. Kumar Bhatt for their comments and assistance. I also must thank the SLD Tau Data Group, with special thanks to Dr. Mourad Daoudi, the head of the group, and to Jim Quigley, who answered endless series of questions from me. I also must express my gratitude to the other members of the SLD Lepton Asymmetry Subgroup: Dr. Robert Panvini, Dr. Terry Reeves at Vanderbilt University (who started Dr. Kroeger and me on this analysis) and Dr. John Harton and Michael Smy at Colorado. Finally, I must thank my parents, Dr. Lee Bolen and Modine Bolen, for keeping me sane through this process.

Abstract

A measurement of the electroweak asymmetry parameter A_t is presented using $e^+e_{LR}^- \rightarrow \tau^+\tau^-$ events from the 1993, 1994-95 data runs at the SLD experiment at SLAC. The analysis takes advantage of the polarized electron beam in the SLAC Linear Collider (SLC) to improve the precision of the analysis over the standard forward-backward asymmetry techniques.

Table of Contents

List of Tables

List of Figures

Introduction

A basic assumption of the standard model is that all generations of leptons couple to the Z^0 boson with the same strength. This concept is known as lepton universality. One means of testing this tenant is to measure this coupling indirectly by measuring the electroweak asymmetry for all three generations of leptons and comparing the asymmetries for each. So due to lepton universality, these asymmetries should be measured to be equal. A brief discussion of the standard electroweak theory and the electroweak asymmetry is given in chapter 1.

This thesis examines the electroweak asymmetry for the heaviest lepton, the tau. This measurement was made using the 1993 and 1994-95 data sets from the SLAC Large Detector (SLD) at the Stanford Linear Accelerator Center (SLAC). Two methods were used to make this measurement. The first method used to measure this asymmetry was left-right improved forward-backward asymmetry technique and the second method used was a log likelihood measurement. Chapter 2 discusses both the detector and the accelerator facility itself. Chapters 3 and 4 discuss the purification of the data sample, the two measurement techniques, and corrections placed upon the measurement. Finally, the two measurements are compared with each other, with the 1995 combined LEP value, and the current SLD measurement of the electroweak asymmetry for the electron.

Chapter 1
Weak Field Theory and the Electroweak Asymmetry

1.1 A Brief Summary of Weak Field Theory

A major triumph of the Weinberg-Salam-Glashow standard model of fundamental interactions was the unification of the electromagnetic and weak forces. Until the development of the standard model these were thought of as two independent forces, each obeying its own set of rules.

Quantum effects for the electromagnetic interaction between matter and light are correctly described by quantum electrodynamics (QED). The first formulation of the theory was proposed by P. A. M. Dirac in 1927. It was able to predict first order effects such as Compton scattering and Bhabba scattering but when it was taken to higher orders, infinities were encountered. The first covariant formulation of QED was developed by Freeman Dyson, Richard Feynmann, Julian Schwinger, and Sin-itiro Tomonaga during the 1940's. This formulation of the theory had the advantage that it was renormalizable, thus it was able to handle the infinities which had plagued Dirac's formulation of the theory. It described the interaction between two vector quantities: the electromagnetic current (j_α) and the electromagnetic potential (A_α). The interaction QED hamiltonian (which combines Dirac and Maxwell fields) has the form:

$$H_{QED} = j^\alpha A_\alpha . \qquad (1.1a)$$

The electromagnetic current is defined as $j^\alpha=-es^\alpha$, where s^α is the Dirac field symmetry current and e is the charge on an electron.

$$s^\alpha = \overline{\psi}(x)\gamma^\alpha\psi(x). \tag{1.1b}$$

So the interaction QED hamiltonian is

$$H_{QED} = -e\overline{\psi}(x)\gamma^\alpha\psi(x)A_\alpha(x)\,. \tag{1.1c}$$

QED was extremely successful. By taking the hamiltonian to second and higher order, QED is able to correctly predict Bhabba scattering, pair production, Compton scattering, the Lamb shift, as well as many other processes.

The weak force first manifested itself in radioactive beta decay. The first explanation of beta decay was postulated by Fermi in 1934.[1] He (correctly) used Pauli's neutrino hypothesis to explain missing energy in the decay of the proton. Like QED, Fermi described the weak force as a vector interaction. In QED, a fermion current is coupled to the electromagnetic field. But in Fermi's theory, the two fermion currents are coupled directly together, thus his hamiltonian describes a point interaction. Fermi's hamiltonian has the form

$$H_{Fermi} = g\left(\overline{\psi}_n\gamma_\alpha\psi_p\overline{\psi}_\nu\gamma^\alpha\psi_e + \psi_n\gamma_\alpha\overline{\psi}_p\psi_\nu\gamma^\alpha\overline{\psi}_e\right). \tag{1.2}$$

The factor g is a coupling constant which measures the strength of the interaction, and $\psi_n\psi_p\psi_\upsilon\psi_e$ are the wave functions for the neutron, proton, neutrino, and electron respectively. However, Fermi's theory was valid only to first order because infinities were encountered when it was calculated for higher orders. Thus, it was known not to be the final theory describing the weak interaction.[2]

In 1956, T. D. Lee and C.N. Yang showed that theoretically there was no reason to expect weak interaction to conserve parity. The first evidence of parity violation was in an experiment by C.S. Wu and her coworkers at the National Bureau of Standards.[3] Subsequent experiments by R. Garwin, L. Lederman and M. Weinrich[4] at Columbia, and J. I. Friedman and V.L. Telegdi[5] confirmed Wu's observation of parity violation in the weak interaction.

By 1957, two experimental facts were known about the weak decay. First it was short ranged, thus implying that a massive propagator carried the weak force. Second, the weak decay violated parity so a vector theory (such as Fermi's) would not describe the interaction properly.

Theoretically, it was generally thought that the form of the Lagrangian had to be $J^\mu A_\mu$ as it was in QED not $J^\mu J_\mu$ like in Fermi's theory, but it had to reduce to Fermi's theory in the low energy limit.[6]

The parity violating nature of the weak decay implied that Fermi's theory of the weak interaction needed to be modified, so that it too would be

parity violating. This was done by Sudarshan, Marshak, Gell-Mann, and Feynmann during the late 1950's. They proposed that the leptons were coupled with their neutrino counterparts to form the leptonic current, with the coupling given by $\gamma_\alpha(1-\gamma_5)$ instead of γ_α (as was the case for QED and Fermi's original theory). So. the weak current is written as

$$J_\alpha(x) = \sum_l \overline{\psi}_l(x)\gamma_\alpha(1-\gamma_5)\psi_{\upsilon_l}(x). \tag{1.3}$$

Note that in the current, there is a vector term, $\overline{\psi}_l(x)\gamma_\alpha\psi_{\upsilon_l}(x)$, and pseudo-vector term, $\overline{\psi}_l(x)\gamma_\alpha\gamma_5\psi_{\upsilon_l}(x)$. Thus, this current is often referred to as a V - A current (vector minus axial vector current). When the the two terms are combined, they form a parity violating current.[7]

Also during this same period, Yang and Mills proposed the idea of using local symmetry to construct gauge field theories. Earlier gauge theories had the disadvantage that the symmetries of the fields had to be global over all space and time, but Yang and Mills had a new concept. They proposed that the symmetries obeyed by the current only had to be local to one point in space-time. When the fermion current is coupled to a gauge field, it regains its global symmetries.[8]

However, the Yang-Mills gauge theory had a major difficulty. This was that the gauge fields that it produced were massless. This problem was solved in 1963 by Peter Higgs. He used Goldstone's concept of spontaneous symmetry breaking to enable the gauge fields to gain mass.[9]

In 1967 Weinberg and Salam, proposed that the weak interaction be invariant under a SU(2) x U(1) transformation. These gauge transformations represent the doublet state for left handed leptons (containing both the lepton and its neutrino) and two singlet states for right handed states (one for the lepton and one for its neutrino). By forcing the equations to be invariant under these two symmetries and taking into account that there are no right handed neutrinos in nature; two conserved charges were found: the third component of the weak isospin (I_3) and the hypercharge (Y_w). These two new charges are related to the electromagnetic charge as $Q = I_3 + \frac{Y_w}{2}$. As Yang-Mills theory demands, this SU(2)xU(1) invariant gauge theory produced four gauge bosons (W_1,W_2, W_3 and B). The intermediate vector bosons actually observed in nature are defined in terms of these four gauge fields (W_α, B) and by the Weinberg weak mixing angle (θ_w) as

$$\begin{aligned} W^{\pm} &= \frac{1}{\sqrt{2}}\left[W_1 \mp iW_2\right] \\ Z &= W_3\cos\theta_w - B\sin\theta_w . \\ A &= W_3\sin\theta_w + B\cos\theta_w \end{aligned} \qquad (1.4)$$

By applying these gauge symmetries, the following interaction Lagrangian was found:[10]

$$L_I = L_{EM} + L_{\substack{Charged \\ Weak}} + L_{\substack{Neutral \\ Weak}} \qquad (1.5\ a)$$

where

$$L_{EM} = -s^{\mu}(x)A_{\mu}(x) \tag{1.5 b}$$

$$L_{\substack{\text{Charged}\\\text{Weak}}} = -\frac{g}{2\sqrt{2}}\left[J^{\mu\dagger}(x)W_{\mu}(x) + J^{\mu}(x)W^{\dagger}{}_{\mu}(x)\right] \tag{1.5 c}$$

$$L_{\substack{\text{Neutral}\\\text{Weak}}} = -\frac{g}{\cos(\theta_w)}\left[J^{\mu}(x) - \frac{\sin^2(\theta_w)s^{\mu}(x)}{e}\right]Z_{\mu}(x). \tag{1.5 d}$$

Note that this Lagrangian now contains an electromagnetic term, a charged weak current term and a neutral weak current term. Also note that now there are three massless vector gauge fields: W_{μ}, Z_{μ}, and A_{μ} (the photon term).

By then applying Higg's postulate of spontaneous symmetry breaking, these gauge fields may gain mass and become the massive charged $W^{\pm}$ and the neutral Z^{O} weak vector bosons and still leave the familiar photon to be massless. Together these bosons with three generations of leptons and the yet undiscovered Higgs particle(s) compose the standard electro-weak model.

Finally, an SU(3) group representing the strong force which is governed by the laws of quantum chromodynamics (QCD) is added to the SU(2)xU(1) structure described above. So, three generations of quarks together with eight colored gluons are added to the electro-weak model. This SU(3)xSU(2)xU(1) structure is the standard model which was developed by Glashow-Weinberg and Salam in 1973.

1.2 The Electroweak Asymmetry and Lepton Universality

As discussed in section one of this chapter, the neutral electroweak interaction is composed of two competing processes, one is the electromagnetic term, which is mediated by a photon and the other is the weak which is mediated by a

Electroweak Processes

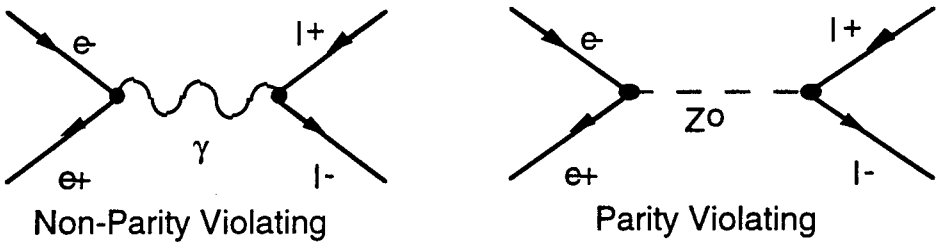

Figure 1.1

Z^0. (see figure 1.1) Thus, the process mediated by a photon gives rise to a non-parity violating term in the cross section while the process mediated by the Z gives rise to a parity violating term.

Normally the electromagnetic term dominates over the weak interaction. However, in the experiment used for this thesis, the electrons collide at the resonance of the Z^0, so that this parity violating term will dominate. This enables SLD to perform a variety of precision measurements of the parity violating process.

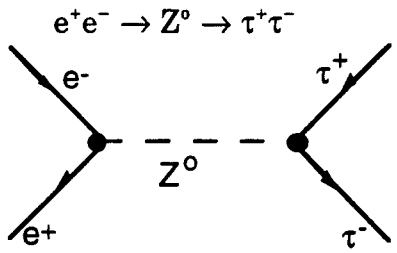

Figure 1.2

Because of the Z^O's huge mass, it has many decay modes. The specific process which this thesis examines is $e^-_{L,R}e^+ \rightarrow Z^o \rightarrow \tau^+\tau^-$ (see figure 1.2), where the notation $e_{L,R}$ denotes an electron of either left or right handed helicity. The cross section for this process is given as

$$\frac{d\sigma}{d(\cos(\theta))} \propto (1+PA_e\delta_{LR})(1+\cos^2(\theta))+2(P\delta_{LR}+A_e)A_\tau\cos(\theta). \qquad (1.6)$$

δ_{lr} is +1 for a left handed beam and -1 for a right handed beam, P is the magnitude of the longitudinal polarization of the beam and A_e and A_τ are the asymmetries of the electron and the tau respectively and θ is the angle of the outgoing τ^- to the beam axis. The magnitude of the electron beam's polarization is defined as:

$$P = \left|\frac{N_{Left} - N_{Right}}{N_{Left} + N_{Right}}\right|. \qquad (1.7)$$

N_{Left} and N_{Right} are the number of left and right handed electrons, respectively. For example, an 80% left handed polarized beam would have 80% of the electrons are polarized left handed and 20% of the electrons are unpolarized. Thus, on average, 90% of the electrons in this beam would

have a left handed helicity and 10% of the electrons would have a right handed helicity. Note that the cross section (eqn. 1.6) has one term which is symmetric with respect to θ and another which is asymmetric in θ.

The coupling strength of the electron to the Z^0 has been measured very precisely by SLD and the various experiments at LEP, so by measuring the electroweak asymmetry for the tau, information can be obtained on the coupling strength between the tau and the Z^0. According to electroweak theory, this strength should be the same for all leptons, thus the asymmetries for each generation should be equal.

$$A_e = A_\mu = A_\tau \tag{1.8}$$

Thus the measurement of the tau asymmetry could be used as a cross check on lepton universality.

The asymmetry parameter for leptons may be alternately written in terms of the axial vector and vector coupling constants or the Weinberg angle as

$$A_l = \frac{2 g_v^l g_A^l}{\left(g_v^l\right)^2 + \left(g_A^l\right)^2} = \frac{2\left(-\frac{1}{2} + 2\sin^2\theta_w\right)\left(-\frac{1}{2}\right)}{\left(-\frac{1}{2} + 2\sin^2\theta_w\right)^2 + \left(-\frac{1}{2}\right)^2}. \tag{1.9}$$

By measuring the cross section for all hadronic events*, SLD has used the polarized beam to make precision measurements of the electroweak asymmetry for the electron by measuring the left-right asymmetry as

$$A_{LR} = \frac{\sigma_L - \sigma_R}{\sigma_L + \sigma_R} = |P| A_e . \tag{1.10}$$

σ_l and σ_R are the measured cross sections for right and left handed polarized electron beams and P is simply the magnitude of the polarization of the electron beam.

A similar procedure was performed in the measurement of the asymmetry for the tau lepton. The left-right improved forward-backward asymmetry was measured as

$$\tilde{A}_{FB} = \frac{(\sigma_{LF} - \sigma_{LB}) - (\sigma_{RF} - \sigma_{RB})}{(\sigma_{LF} + \sigma_{LB}) + (\sigma_{RF} + \sigma_{RB})}. \tag{1.11}$$

σ_{rf}, σ_{rb}, σ_{lf} , and σ_{lb} are the cross sections for left, and right events which are going in the forward and backward directions. Left and right refer to the sign of longitudinal polarization of the incident electron. Forward and backward refer to the direction of the final state lepton (in this case the tau). If the τ^- is moving in the same direction or if it is in the same hemisphere as the initial e^- (θ less than 90^o) then this is classified as a forward event, however if the τ^- is moving in the opposite direction or hemisphere from the

* Along with a 10% tau contamination

e^- (θ greater than 90^o) it is classified a backward event. These event topologies are summarized in figure 1.3.

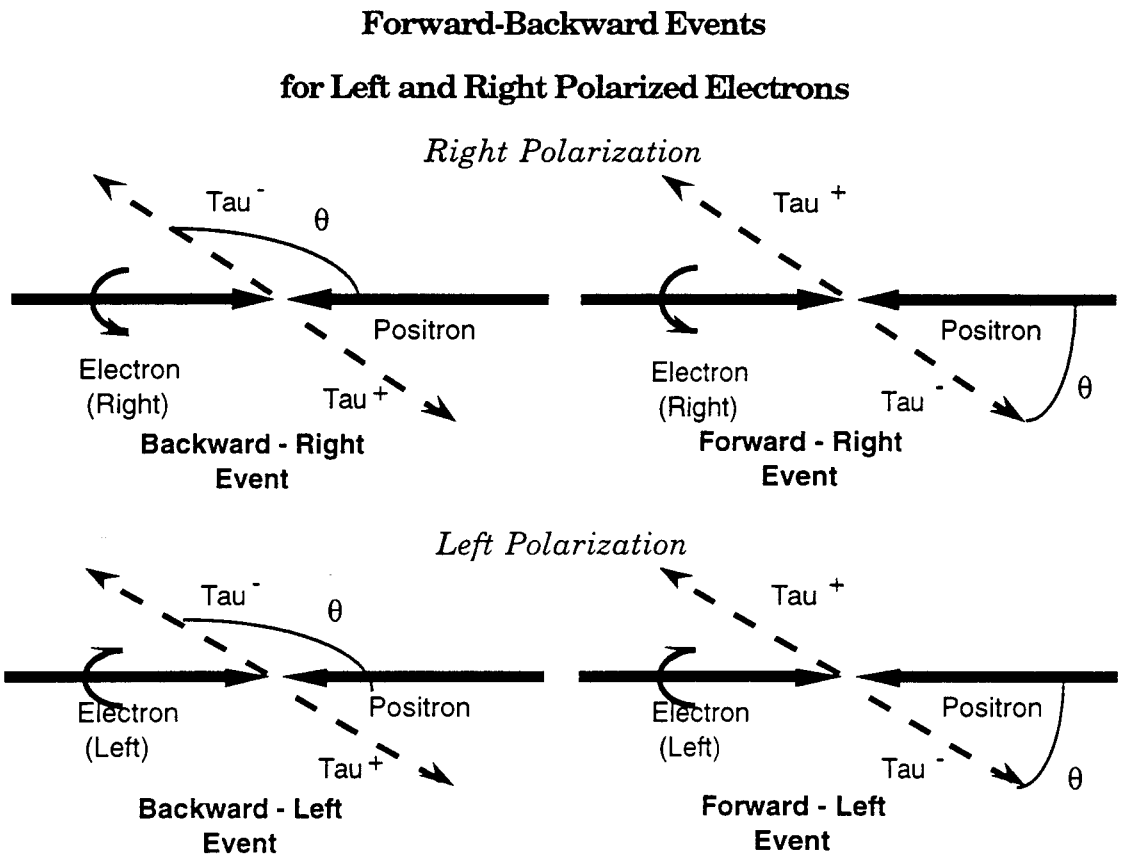

Figure 1.3

The left-right improved forward-backward asymmetry is related to the electroweak asymmetry as

$$\tilde{A}_{FB} = \frac{3}{4}|P|A_\tau \qquad (1.12)$$

where P is the polarization, so by measuring the left-right improved forward-backward asymmetry, one may find the electroweak asymmetry for the tau.

Chapter 2
Description of SLD and SLC

2.1 Stanford Linear Collider

The Stanford Linear Collider (SLC) is a electron-positron collider at the Stanford Linear Accelerator Center (SLAC). The SLC was built as an extension to the existing linear accelerator. The SLC was completed in 1989. The first Z^0 events were recorded with the Mark II detector. In 1991 the SLAC Large Detector (SLD) replaced the Mark II and first began taking data in 1992.

Both the electron and positron beams have an energy of 46.6 GeV.[1] (varying slightly from year to year) The SLC is operated slightly off the Z^0 resonance (the Z^0 has a mass of 91.187 ± 0.007 GeV)[2] because the SLC polarization depends upon the energy and the particle trajectories. The beam is tuned so that the uncertainty in SLD's eventual measurement of A_{LR} is minimized. This is done by maximizing the factor - $P^2 \frac{dN_{Z^0}}{dt}$ (polarization squared times the Z^0 production rate).

$e^-e^+ \rightarrow Z^0$ at the Z^0 resonance is also studied at the four experiments at the European accelerator: LEP (Large Electron Positron Collider) at CERN with a much greater luminosity than SLC. The major difference between the SLC and LEP is the topology of the two colliders. As SLC's name

implies, it is a linear collider. This is in contrast with LEP, which is a storage ring.

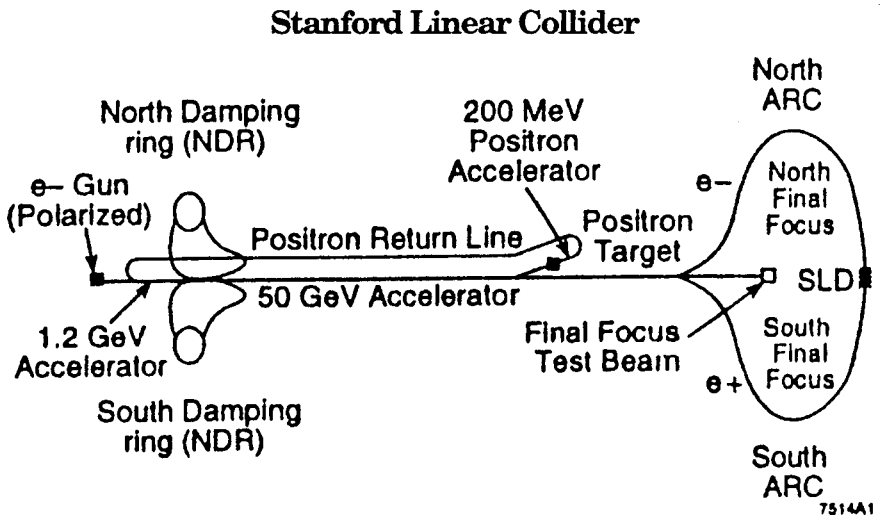

figure 2.1

At LEP, the electron and positron bunches orbit the main storage ring on the order of 10^5 times per sec, thus allowing for many chances of interaction. The problem with this method of accelerating electrons is that they have such a small mass that much of the energy which is given to the electrons in acceleration is radiated off in the form of synchrotron radiation. The SLC, on the other hand, only allows the bunches to collide once, thus reducing the power needed to compensate for synchrotron radiation, but at the same time only allowing one chance for an interaction. More specifically, the cost of building and operating a storage ring collider (such as LEP) are proportional to the square of energy of the beams. On the other hand, a linear accelerator's cost is only linearly proportional to its

energy. Thus, SLC may become the first of a new generation of linear electron - positron machines.

The process of creating and accelerating the beams to collide with a center of mass energy of 92 GeV is accomplished in several stages. First, two polarized electron bunches of 2-3 x 10^{10} electrons are produced by the polarized electron source with a repetition rate of 120 Hertz. One of the electron bunches is accelerated to 30 GeV and then diverted into a tungsten-rhenium target, where the electrons produce a shower of photons. Some of the photons pair produce, and so via a magnetic field some of the resulting positrons can be swept into a return line and transported back to the start of the LINAC. The remaining two bunches of e^+ and e^- are then transported to an electron or positron damping ring, respectively, in order to "cool"* each bunch to a uniform energy.

After the two bunches are cooled in the damping rings, they are returned to the two mile long linear accelerator where they are accelerated to 46.6 GeV. The polarized electrons are swept into the left arc, and the positrons are swept into the right arc.[3]

Finally, the beams are then brought into tight focus by the final focus magnets at the interaction point inside the center of the SLD detector. At the interaction point, they have a 2.6 x 0.8 micron^2 spot size. The interacting particles produce Z^0 bosons at rest, as discussed above. This

* Cooling the electron beam is the process of placing the bunch of electrons in a small ring then via sychrotron radiation all of the electrons with higher energy will radiate their energy faster than the electrons with less energy. So, the electrons will tend toward the same energy over time.

extremely narrow and stable interaction point allows SLD to have extremely accurate vertex detection.

The overwhelming majority of the beam particles pass each other without interacting, they are then extracted into the beam lines where their energies and the degree of polarization of the electron bunches are measured, and then they are disposed of in the beam dump.

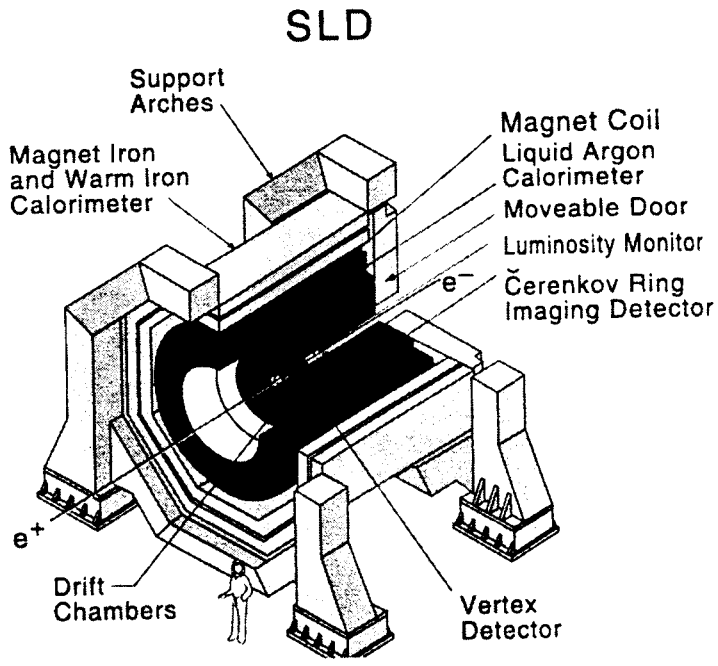

figure 2.2

- 2.2 Beam Polarization

A second distinction between the SLC and its European counterpart is that the electron beam's spin is longitudinally polarized in the SLC. The actual degree of polarization in the beam at SLC has been steadily increasing; from 20% in 1992 to almost 80% during the 1994-1995 data run.

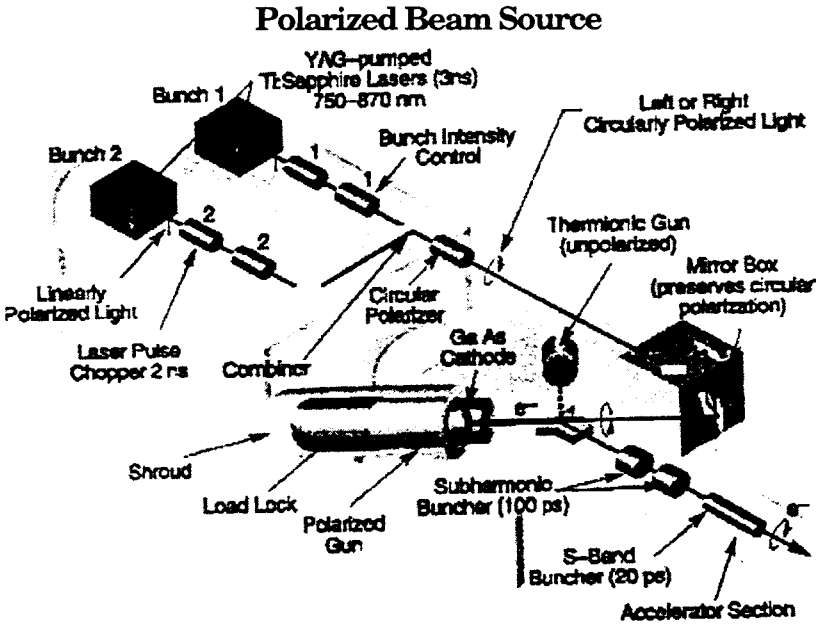

Figure 2.3

The polarized electron beam is created by directing a beam of circularly polarized laser light onto a GaAs semiconducting cathode. The energy of the oncoming photons is slightly greater than the energy gap of the GaAs cathode. There are two transitions in the GaAs which can be excited by this photon. The Clebsch-Gordon coefficients show that there is a 3:1 ratio between these two transitions. More specifically, the number of times

electrons are excited by right handed photons from the $P_{3/2}\left(m_j = -\frac{3}{2}\right)$ valence band to the $S_{1/2}\left(m_j = -\frac{1}{2}\right)$ conduction band giving the electron a left handed spin is three times as likely as a right handed photon exciting electrons from the $P_{3/2}\left(m_j = -\frac{1}{2}\right)$ valence band to the $S_{1/2}\left(m_j = \frac{1}{2}\right)$ conduction band giving the electron a left handed spin. A similar argument holds for a left handed photons, they causes the emission of a right handed electron verses right handed electrons in a 3:1 ratio. So there is a theoretical limit of 50% $\left(\mathrm{P} = \frac{3-1}{3+1}\right)$ polarization of the electrons emitted from the cathode. But by placing a strain on the GaAs lattice, this degeneracy between the two energy levels in the $\mathrm{j} = \frac{3}{2}$ state is removed and this limit to the degree of polarization of the outgoing electrons may be in theory improved to 100%. In reality however, the cathode with the strained lattice has shown a polarization of 80%.[4]

The spin of the polarized electron is carefully maintained by SLC during its acceleration down the linac. By taking advantage of a resonance in the arc, the electron's spin precesses while it sweeps around the arc and is rotated so it's spin axis is along the beam axis as it enters the interaction point inside the SLD.

2.3 SLAC Large Detector

The SLAC Large Detector (SLD) is located at the interaction region of the two beams (see figure 2.2). One quadrant of the detector is shown in a schematic cutaway view in figure 2.4.

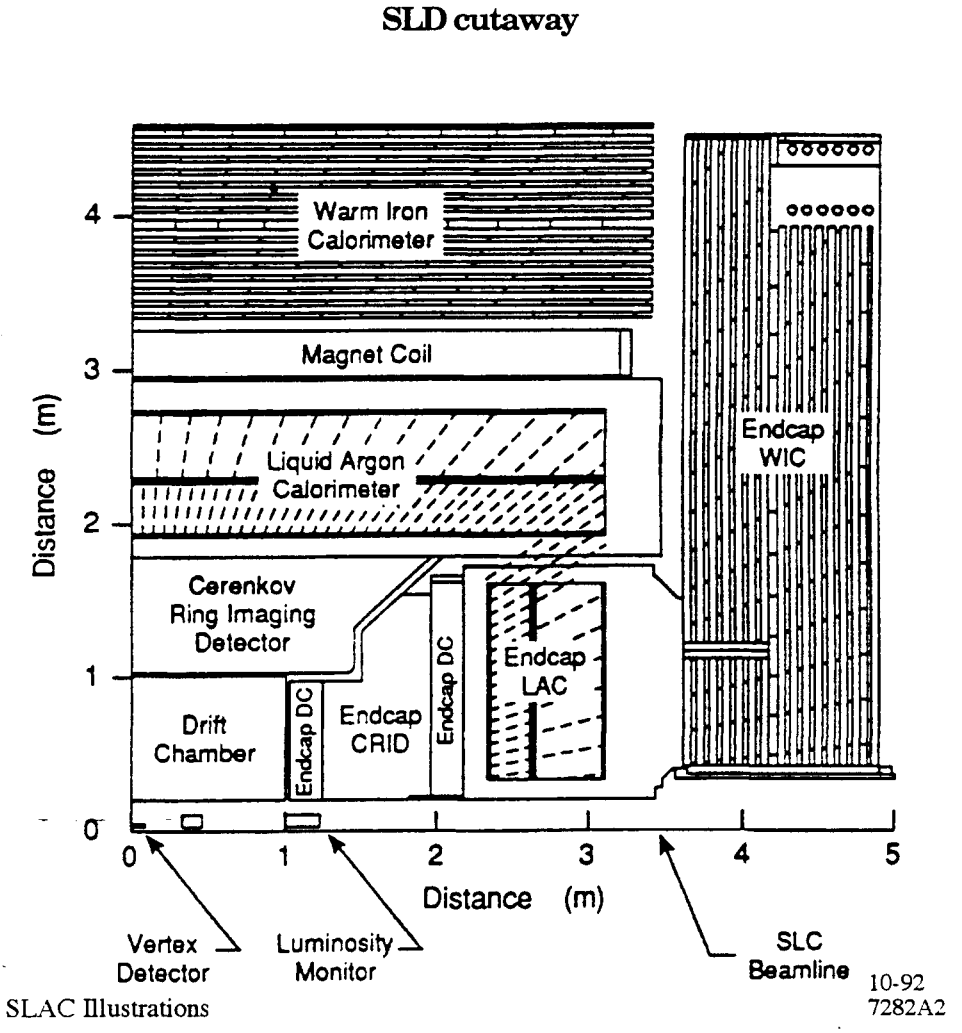

Figure 2.4

2.3.1 Vertex Detector

At the center of the detector is the vertex detector. It is a cylinder surrounding the interaction point with a radial distance of about 3 to 4 cm from the interaction point and is 9 cm long. The vertex detector uses CCD's (Charged Coupled Devices), the same silicon chips which are used in home video cameras.[5] Each CCD is comprised of a 222x530 array of silicon pixels on the surface of the detector. Each pixel has an area of 22x22 microns. As a charged particle passes through these silicon layers, it ionizes the silicon creating electron hole pairs. The net charge on each pixel of a row on the CCD is measured, then by using an electric field the row is shifted so that the next row may be read out. The process of measuring the charge on all the rows on the CCD takes around 50 msec.[6]

Vertex Detector

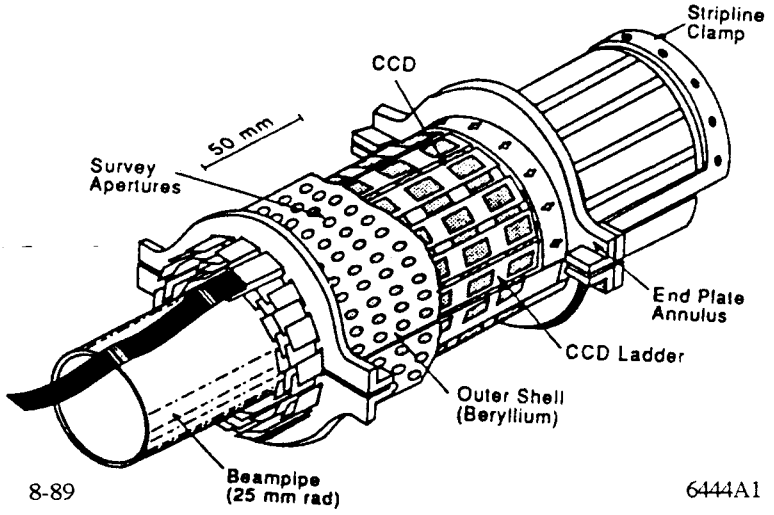

Figure 2.5

These CCD's are mounted on both side of ladders which are 1 CCD wide and 6 to 8 CCD's long. These ladders are then placed into 4 overlapping

nested barrels. The ladders overlap from one barrel to the next such that any particle emerging from the primary vertex with a polar angle less than 29 degrees must pass through two of the ladders. The entire vertex detector is cooled to -80° C with nitrogen gas in order to reduce the effects of noise from thermal excitations and loss of CCD charge-transfer efficiency due to radiation damage. Together these ladders are able to measure a track to within 5 microns at the interaction point.[7]

2.3.2 Central Drift Chamber (CDC)

Around the vertex detector are the Central Drift Chamber (CDC) and the Endcap Drift Chamber. The CDC is a 2 meter long cylinder. It has an inner radius of 0.2 m, and an outer radius of 1.0 m. The drift chambers are filled with a gas consisting of carbon-dioxide, argon, isobutane and trace amounts of water. Inside the chamber are a series of high voltage wires and wires connected to charge amplifiers (known as sense wires). As charged particles pass through the gas, they ionize it. The free electrons, having much less mass than the resulting ions themselves, drift toward the positive high voltage wire. As the ionized electron approach the sense wires, they have enough kinetic energy to produce a cascade of electrons in the gas. These cascade electrons then drift toward the sense wire, producing a signal which is amplified, digitized, and read out. The sense wires detect this cascade. The wires are staggered to resolve left-right ambiguity as to which side of the wire that the charged particle passed. The CDC is composed of eighty layers of wires which are in a 0.6 Tesla

magnetic field. It has a resolution of about 100 microns. The CDC can resolve two tracks as close as 1 mm apart.[8] The CDC has an inverse momentum resolution of $\sigma^2\left(\frac{1}{\mathrm{GeV}}\right)=\left(\frac{0.0050}{p}\right)^2+(0.0050)^2$.[9]

- *2.2.3 Cerenkov Ring Imaging Detector (CRID)*

After the particles pass through the CDC, they pass through the main barrel and endcap Cerenkov Ring Imaging Detector (CRID). This is used for final state particle identification. It is well known that as a charged particle passes through matter traveling faster than the speed of light in that medium, a cone of light is emitted. This is called Cerenkov radiation. The opening angle of the cone of Cerenkov light is dependant upon the velocity of the particle relative to the speed of light in the medium. The angle of emitted light as a function of the particle's velocity is given as

$$\cos(\theta) = 1/\beta n \qquad (2.1)$$

where $\beta=v/c$ and n is the index of refraction of the medium that the charged particle is passing through.

In order to detect particles over the entire momentum range, the CRID uses both a liquid (C_6F_{14}) and a gas (C_5F_{12}) Cerenkov radiators. The particle first traverses a thin layer of the liquid and the resulting Cerenkov cone is imaged as a ring onto the detector box. The charged particle then passes through the detector box and into the gas radiator. The resulting Cerenkov cone in the radiator gas is then also imaged onto the detector box

via parabolic mirrors. These two rings of Cerenkov photons from the liquid and gas radiators then pass through quartz windows at the back and front of the detector box respectively. In the detector box, they are then converted to electrons by photo-ionizing TMAE (Tetrkis-Dismethyl-Amino-Ethane) gas which was chosen for its very high quantum efficiency for the expected wavelengths of Cerenkov light. These photo-electrons then drift into a set of proportional wire detectors where both the drift time and the position of the wire hit is recorded. So the detector can measure the size of the rings and hence the opening angle of the two cones may be determined. By using this information in conjunction with the drift chamber's measurement of the particle's momentum, the charged particle's species can be identified.[10]

2.3.4 Liquid Argon Calorimeter (LAC)

Almost a third of the resulting particles from the Z^0 decay are neutral (mostly photons from π^0 decays). In order to detect these particles it is necessary to stop them in matter and measure their energy. This is done in the LAC (Liquid Argon Calorimeter). Like the CDC and the CRID, it too is composed of both a barrel and an endcap section. The two chambers are designed to be almost fully hermetic and the barrel and endcaps cover 98% of the full solid angle. The LAC is constructed of cells consisting of lead tiles separated by plastic spacers. Liquid argon fills the gap between the layers of tiles. Each of the particle types have different signatures in the LAC.

- High energy electrons and photons interact with the electromagnetic field of the lead nuclei. This interaction causes the electrons to emit bremsstahlung radiation, and causes the high energy photons to pair produce. These processes are repeated for the particles resulting from the primary interactions causing an electromagnetic cascade of particles in the calorimeter. This process of showering eventually stops once the energies of the resulting particles are below the necessary threshold energies of these production mechanisms.[11]

- Charged and neutral hadrons collide with the lead and argon nuclei. Since this is a strong interaction, it produces a high multiplicity of particles. So just as in the case for electrons and photons, a shower is produced inside the calorimeter. However a hadronic shower is much more complex than its electromagnetic counterpart because of the greater variety and higher multiplicity of particles. Many of the secondary particle are π^0's, which then produce two photons. These photons interact electromagnetically. Unfortunately, a reasonable fraction of the energy of the hadron is never detected because it is used in the break up of the target nuclei. Other decay products include charged particles which, in turn ionize the liquid argon, making the energy clusters used in identification of particles. Thus, hadronic calorimetry is much more complex than electromagnetic calorimetry.[12]

- Muons, although charged, have too great a mass to give rise to much bremsstruhlung radiation, but instead they traverse the LAC leaving small

depositions of energy which are characterisic of minimum ionizing particles.

- Unfortunately, neutrinos have such a small cross section for interaction with matter, that they escape the LAC undetected.

The calorimeter is divided into four sections. First the particles travel through two electromagnetic (EM) parts where the lead is thin (2 mm) and are designed to measure electrons and photons. The remaining two sections of the LAC have thicker lead tiles (6 mm) and provide the nessary mass to contain hadronic showers. The LAC is thick enough to contain 95% of the hadronic energy.

This design was used so that the LAC would have good energy resolution and a fairly flat uniform response for both electromagnetic and hadronic showers. The energy resolution for electromagnetic showers is $10-12\%/\sqrt{E(GeV)}$ and for hadrons it is $60\%/\sqrt{E(GeV)}$.[13]

In order to detect the ionized electrons in the argon bath, every second lead plate is raised to a high voltage. So as in the drift chamber, a cascade is produced which sweeps the ions onto the uncharged lead tiles. The tiles along the same radial directions are grouped together to form towers. The detector's resolution is limited by statistical fluctuations in the ionization charge deposited in the sensitive regions and because the fluctuations are different for electromagnetic and hadronic showers, the LAC's energy resolution differs for these two processes.

- 2.3.5 *Magnetic Coil*

Outside the LAC is the magnetic coil. The magnet is a 0.6 Tesla room temperature aluminum solenoidal coil.[14] The limit of the momentum resolution of the detector is directly proportional to the coil's magnetic strength.[15] This magnetic fields allows the tracking to have a momentum resolution of $\left(\frac{\delta p_T}{p_T}\right)^2 = 0.13 \times 10^{-3}\left(\frac{GeV}{c}\right)^{-1}$.[16]

- 2.3.6 *Warm Iron Calorimeter (WIC)*

Beyond the magnetic coil is the WIC (Warm Iron Calorimeter). Like the CRID and the LAC, the WIC is composed of a barrel and two endcap sections. This consists of 18 layers of Iarroci gas tubes which are placed between one inch plates of steel. The Iarroci tubes are filled with a mixture of 88% CO_2, 9.5% isobutane, and 2.5% argon gases, and are painted inside with a slightly conductive carbon paint.[17] A high voltage wire is placed inside the tube. When a charged particle ionizes the gas, the electrons are attracted to the wire, and the positive ions are repelled to the surface of the tube. Thus a small charge can be measured on the side of the Iarroci tube. The WIC was intended for the dual purpose of muon tracking and to catch the remaining energy from hadronic showers that passed through the LAC, but it is now solely used for muon tracking. The WIC is very effective at muon tracking and is able provide enough resolution along the axis of SLD to measure these coordinates to ≤ 10 mrad.[18]

- 2.4 Luminosity Monitor

The integrated luminosity of the two beams is found by measuring the rate of low angle predominately t-channel Bhabha events (electron-positron scattering) in the SLD detector. This measurement is made by the luminosity monitor/small angle taggers (LMSAT).[19] These are two silicon calorimeters which are located 100 cm on either side of the Interaction point of the two beams. The calorimeters cover the angular region of 28 mrad to 65 mrad measured from the beam axis. Each calorimeter has six radial sections. A single radial section has 23 alternating layers 3.5 mm thick plates of tungsten alloy and 300 μm layers of silicon diodes. The LMSAT is able to contain 99.5% of the scattered electron's energy. Both calorimeters have an energy resolution of $\sigma(E)/E = 20\%/\sqrt{E}$.[20]

- 2.5 Measurement of electron polarization

As the electron beam passes out of the interaction point, the polarization of the electron beam is measured with a Compton polarimeter. The Compton polarimeter is composed of a 532-nm frequency doubled YAG laser which is circularly polarized by a Pockels cell and an electron spectrometer. More specifically, the circularly polarized 32 eV photons from the laser intersect the electron bunch 33 meters downstream from the SLD interaction point. Some of the polarized electrons are scattered by the photons via the Compton effect. The back-scattered Compton electrons are then detected by a series of Cerenkov and proportional tube detectors, enabling a the full Compton scattering rate to be measured as a function of

angle. By measuring the this scattering angle, and knowing the difference in the e-γ cross section for the two spin states of the electron and the two helicity states of the photon, the electron's polarization can be obtained.[21] The differential cross section for Compton scattering of polarized photons and polarized electrons is

$$\frac{d\sigma}{dE} = \frac{d\sigma_u}{dE}\left[1 + P_\gamma P_e A_c(E_s)\right]. \tag{2.2}$$

where σ_u is the cross section for unpolarized Compton scattering, P_γ is the polarization of the photon, P_e is the polarization of the electron, E_s is the energy of the scattered electron, and $A_c(E_s)$ is the Compton asymmetry for γ-e^- spins parallel vs. spins anti-parallel.[22] The polarization is actually measured by finding this Compton asymmetry for the difference in counting rates for parallel $R(P_\gamma P_e > 0)$ and anti-parallel $R(P_\gamma P_e < 0)$ beam-photon helicities. This polarization is given by

$$P_e = \frac{1}{P_\gamma \langle A \rangle}\left[\frac{R(P_\gamma P_e > 0) - R(P_\gamma P_e < 0)}{R(P_\gamma P_e > 0) + R(P_\gamma P_e < 0)}\right] = \frac{A_{Compton}^{Measurred}}{P_\gamma \langle A \rangle}. \tag{2.3}$$

$\langle A \rangle$ is the average Compton asymmetry for the energy interval measured by the detector.

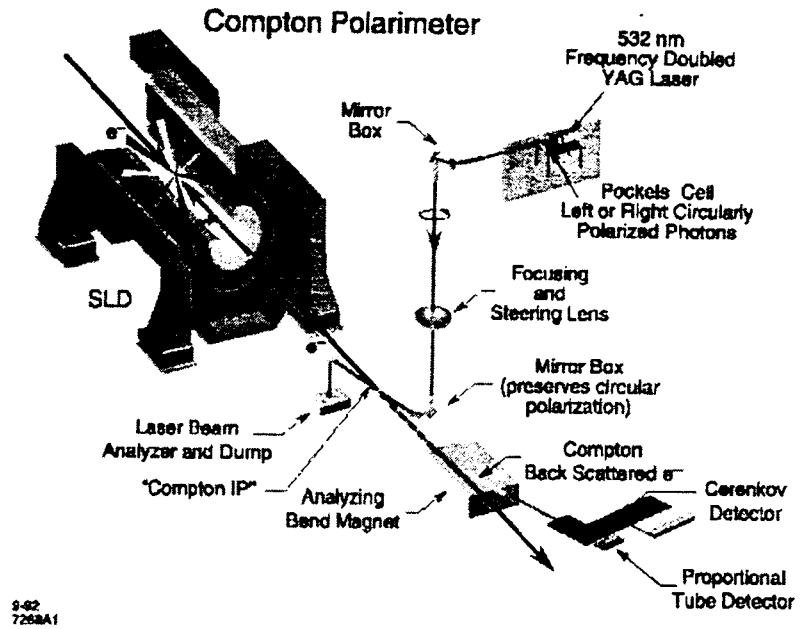

figure 2.6

As the electrons leave the Compton interaction point, they pass through a pair of dipole magnets with a field strength $\left(\int B \bullet dl\right)$ of 3.05 T-m. This field is strong enough to separate the scattered electrons from the electrons that did not interact with the laser. The scattered electrons are bent away from the non-interacting electrons, and enter a detector. This instrument is composed of a set of two multichannel detectors. These two groups of detectors consists of a set of 16 proportional tubes and a set of nine threshold gas Cerenkov detectors. Each Cerenkov detector channel is detecting overlapping bands of energy ranging from 17 to 30 GeV. The proportional tubes are arranged in a horizontal plane thus, also allowing the energy of the scattered electron to be measured. This system of two sets of redundant

momentum measurements allowed the relative polarization of the electron beam to be measured to less than 1%.

The laser is pulsed once every 11 machine pulses. The 10 electron pulses with no laser pulse give an estimate of background from beamstrahlung photons produced at the SLD interaction region. The signal-to-noise ratio is 5-10% for the Cerenkov detectors and 1-2% for the proportional tube detectors.[23]

2.6 Energy Spectrometer

After the electrons and positrons pass through the interaction point and the compton polarimeter, their energy is measured by a pair of energy spectrometers placed at either end of the detector.

Each beam passes through a set of three dipole magnets. The center dipole magnet is an analysis magnet which has a precisely measured magnetic field that causes the beam to deflect from its path by an amount inversely proportional to its momentum. The first and third dipole magnets cause the beam to bend in a horizontal direction which is perpendicular to the vertical bend given to the beam by the analysis magnet. Each bend causes the beam to emit synchrotron radiation. The WISRD (Wire Imaging Synchrotron Radiation Detector) measures the distance between the two horizontal synchrotron strips created when the beam passed through the two bending magnets and so it is able to calculate the

deflection of the beam due to the middle analysis magnet. The energy of the incoming beam can be calculated as

$$E_{beam} = \frac{c}{\theta}\int\left|\bar{B}\times d\bar{l}\right|. \qquad (2.4)$$

where θ is the deflection angle of the beam by the analysis magnet, c is the speed of light, B is the analysis magnet's magnetic field, and dl lies along the beam's path if it were not deflected.[24]

The Energy Spectrometer

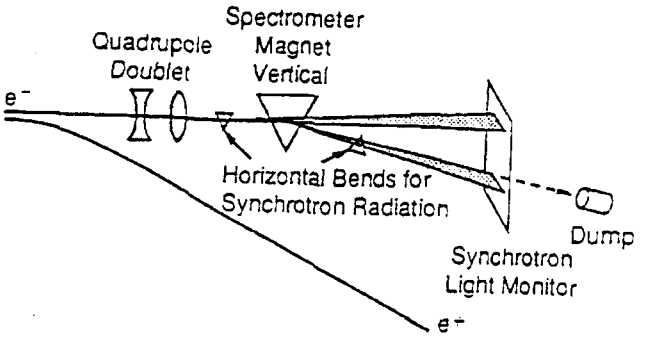

Figure 2.7

The WISRD detector is composed of two grids of copper wires that run parallel to the incoming synchrotron radiation. The array of wires are spaced 100 μm apart and each wire has a diameter of 75 μm. The incident photons from the synchrotron radiation compton scatter off the wires, thus leave a residual charge on the wire. This charge is amplified and measured. This technique allows the separation distance between the two sychrotron radiation strips to be measured to within 0.02%.[25] This

measurement and exact knowledge of the strength and shape of the magnetic field of the analysis magnet allows the mean beam energy to be determined to within 255 ppm or results in an error of 12 MeV for a 45.6 GeV beam.[26]

Once the two beam's energy has bean measured, the beams are dumped.

Chapter 3
Data Acquisition and Purification

3.1 Triggers

The first step in categorizing an event, obviously, is recognizing that one has occurred. This is the function of the trigger. SLD needed an efficient

SLD Triggers

Trigger	Restriction
Energy	LAC energy is greater than 4 GeV
WAB *(Wide Angle Bhabha)*	EM LAC energy is greater than 15 GeV and CDC is ready to take data
LUM *(Luminosity Monitor Bhabha)*	Energy Sum for each LMSAT is greater than 12.5 GeV
Tracking	At least 2 CDC tracks separated by an opening angle of at least 30 degrees.
Muon	WIC strip tracks in opposite octants. *Limited to 0.05 Hz due to background muons traveling with beam.*
Hadronic	At least one CDC track & satisfies energy trigger.
Random	Reads out detector every 2400 beam crossings. (100 sec) Used for background studies.

Table 3.1

and quick (4 msec) method of deciding if a Z^0 event has occurred, so it may write the event to tape for analysis or reject the event entirely. This quick decision is made by SLD by triggers which are described in table 3.1.[1] These triggers produced a rate of around 1 event being written to tape per second.

3.2 Reconstruction of events

The data which passed the trigger are first subdivided into:

- Random Triggers
- Physics Triggers
- Luminosity Monitor Triggers

Physics and Physics Calibration events were further categorized into

- Z Decay Products (includes wide angle Bhabha, muon, tau, and multihadron events)
- Luminosity Monitor Bhabhas
- Track Triggers

The final state fermions were categorized as to tau pairs, electron pairs, muon pairs, and hadronic final states by their signatures in the detector. Tracks in the drift chamber were reconstructed and matched with energy clusters in the LAC and WIC tracks. The identity of the charged particles can be determined by using a combination of drift chambers and the CRID.

But such particle ID has not been employed in this analysis. Next, the events passing those cuts are further constrained by placing quality cuts on these tracks. The events passing this second series of cuts are now fully reconstructed and are now ready for analysis as physics events.

3.3 Selection of Tau Events

Once the event has been reconstructed, the Z^0 decay product candidates must be separated into their respective signatures. The tree-level Feynman diagrams of the various observable Z^0 decay modes are shown in figure 3.1.*

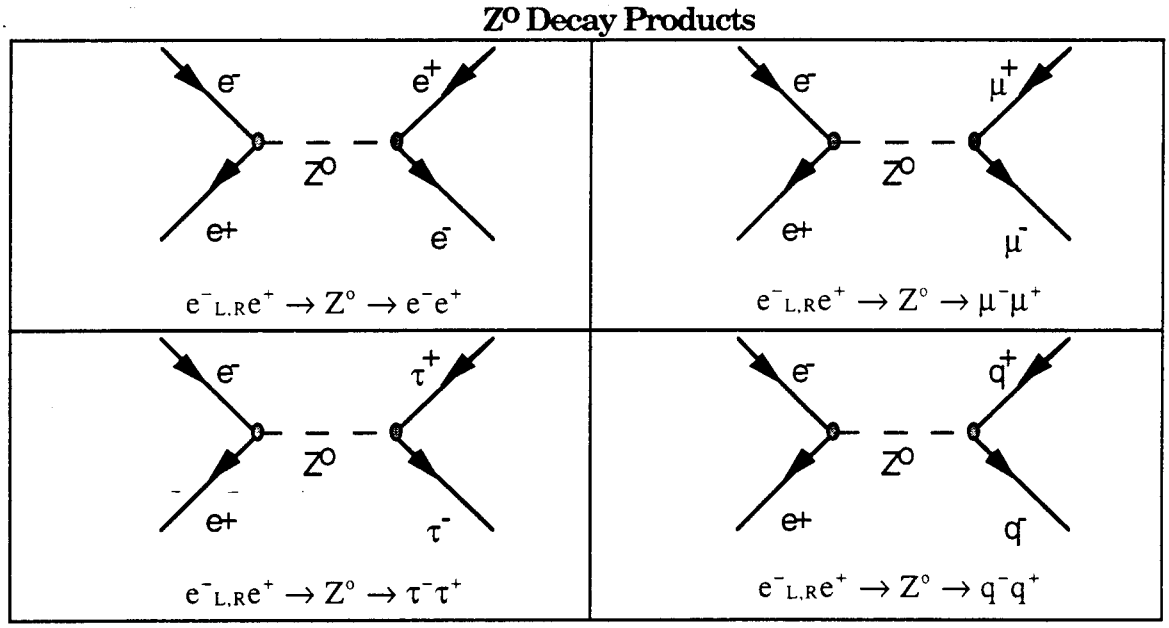

Figure 3.1

These contributions dominate the cross sections for all final states except for e^+e^- at low θ, which are dominated by the t-channel Bhabha term.

* There is a mode of $Z^0 \rightarrow \nu_l\bar{\nu}_l$, but it is unobservable inside the SLD detector since neutrinos penatrate the detector unseen.

In order to analyze the tau decay mode, a clean sample containing only tau decays must be obtained. Hence, the wide angle Bhabha, muonic and hadronic decay modes are background events which need to be removed from the sample. In addition, the SLD data sample contains a small number of so called two photon events (shown below).

Two Photon Event

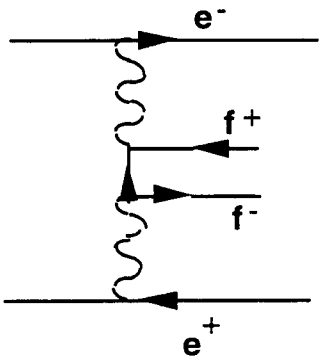

$e^-_{L,R}e^+ \rightarrow Z^\circ \rightarrow e^- e^+ + \text{hadrons}$

Figure 3.2

Common hadronic final states which are created in this process are $\pi^0\pi^0$ and $\pi^0\eta$.[2]

The major signature of a wide angle Bhabha or a muon event is two back to back charged tracks seen inside the detector.

Major Tau decay modes

Decay Mode	Fraction	Decay Mode	Fraction
(1 Prong)	*(85.82 ± 0.25)%*	*(3 prong)*	*(14.38 ± 0.24)%*
$\tau^- \rightarrow \mu^- \bar{\nu}_\mu \nu_\tau$	(17.58 ± 0.27)%	$\tau^- \rightarrow \pi^- \pi^- \pi^+ \nu_\tau$	(5.6 ± 0.7)%
$\tau^- \rightarrow e^- \bar{\nu}_e \nu_\tau$	(17.93 ± 0.26)%	$\tau^- \rightarrow \pi^- \rho^0 \nu_\tau$	(5.4 ± 1.7)%
$\tau^- \rightarrow \pi^- \nu_\tau$	(11.6 ± 0.4)%	$\tau^- \rightarrow \pi^- \omega^0 \nu_\tau$	(1.6 ± 0.5)%
$\tau^- \rightarrow \pi^- \pi^0 \nu_\tau$	(24.0 ± 0.6)%	$\tau^- \rightarrow K^- \pi^- \pi^+ \nu_\tau$	(2.2 ± 1.7)%
$\tau^- \rightarrow \pi^- 2\pi^0 \nu_\tau$	(10.3 ± 0.9)%	*other modes*	*< 0.8 %*

Table 3.2

Analysis of the tau lepton poses some different problems than the analysis of the two lighter leptons. This is because the tau is so short lived that it decays roughly at the interaction point of the colliding beams and the tau (with a mass of 1.784 GeV) is the only lepton heavy enough to decay into hadrons. The average decay length of the highly relativistically boosted tau is 2.19±0.14 mm.[3] Since the vertex detector's inner radius is about 3 cm, the tau, itself, is never observed inside the detector. Instead, the tau's decay products are observed. Some of the energy and momentum of the tau is carried away by neutrinos which pass though the detector undetected. These neutrinos are present in every tau decay in order to conserve lepton number. So instead of seeing two back to back charged tracks in the calorimeter (as one would expect to see for the electron or muon final state), a single track or a small number of grouped tracks (or prongs) are observed on either side of the event. The thrust axes of these two sets of

tracks are acolinear, reflecting the unseen momentum of the neutrinos. What is actually seen in the detector depends on the decay mode of the two taus. However, each group must contain an odd number of tracks in order that their net charge reflects the charge of the tau. The major decay modes of the tau are summarized in Table 3.2. Most of the tau decays have only one charged track but about 15% of the tau decays may contain 3 or more charged tracks.

In order to reflect the physics of the tau decay and to separate the tau sample from the other background events; the SLD Tau working group placed the following restrictions upon the Z^O decay product sample in order to select the tau events. These cuts emphasize purity of the event sample rather than efficiency. In listing the cuts in Table 3.3, the term "jet" is not used in its conventional sense. A "jet" usually refers to a quark or gluon which has fragmented into a collimated group of particles, but its meaning in this context is that a "jet" simply refers to a collimated group of tracks.

The cuts listed in table 3.3 are designed to reflect the physics of the tau decay described earlier in this chapter. As discussed in chapter 2, electrons tend to deposit most of their energy in the electromagnetic section of the LAC. The requirement that less than 45% of the total energy of the decay be within this section of the detector is designed to reduce the number of wide angle Bhabha* events in the sample.

* In this analysis, wide Angle Bhabha events are defined as having the outgoing electron track to have $\cos(\theta)<0.707$

SLD Tau Group Cuts

Quantity	Restriction	Purpose
Visible Energy	greater than 10.8 GeV (12% of the center of mass energy)	Two Photon
Total Energy in the EM section of the LAC	less than 40.5 GeV (45% of the center of mass energy)	Wide Angle Bhabha
Largest Cluster in the EM section of the LAC	less than 30 GeV (33% of the center of mass energy)	Multihadron
Total energy outside a Jet	less than 5 GeV	Multihadron
Number of energy clusters outside of Jets	less than 6 clusters	Multihadron
Angle between track and jet	less than 15 degrees	Multihadron
Acolinearity for multi-prong events	less than 20 degrees	Multihadron
Mass of each Jet	greater than 2.3 GeV	Multihadron
Sum of momenta for largest track	less than 65 GeV	Wide Angle Bhabha Muon Pair
Acolinearity of (1 prong-1 prong) events	greater than 10 mRad	Wide Angle Bhabha Muon Pair
Number of "Good" Tracks	Between 2 and 6	Multihadrons
Angle of missing momentum to beam	Cos θ less than 0.88	Wide Angle Bhabha Two Photon

Table 3.3

As mentioned earlier, one of the distinguishing signatures of a tau event is that some of the momentum is never seen inside the detector since it is carried away by invisible neutrinos. Thus, the tau event is generally characterized by two groups of charged tracks which are slightly acolinear. So, a requirement was placed on 1 prong- 1 prong events not be back to back, helping to eliminate muon and electron pairs.

Another major background which must be reduced in the sample are multihadron events. Multihadronic events differ from tau events in that they tend to have a high multiplicity of tracks within the event. Many of the cuts listed above are designed to reduce this hadronic contamination of the sample. As stated above, the cuts on the acolinearity between tracks is designed to reflect the missing momentum due to the neutrinos in the decay. However, the required acolinearity cannot be too large or multihadronic events will contaminate the sample. This explains the two separate cuts on the upper and lower bounds on the acolinearity of the two maximum momentum tracks. There must be some acolinearity between the two maximum momentum tracks in order to reject electron and muon events, but not enough acolinearity to allow hadronic events to pass the cuts. The requirement that there be less than 6 energy clusters outside of the two "jets" reflects the high multiplicity of hadronic events and therefore reduces the number of background hadrons entering the sample.

Effects of the Tau Groups Cuts

Type	Relative Yield	Efficiency of Tau Group's Cuts	Expected Sample per Tau
Tau	1	0.62	1
Hadronic	20.54	0.00034	0.012
Muons	1	0.0065	0.010
Two Photon	0.66	0.0045	0.0078
Wide Angle Bhabhas	1.1	0.0014	0.00149

Table 3.4

The SLD group cuts gave the efficiencies listed above for several different Monte Carlo samples. These numbers are specific to the recon 11 version of the SLD reconstruction code. For two photon and wide angle, the yields

and efficiencies cited are only defined relative to some choices of parameters in the Monte Carlo generation, but the product in the last column should be meaningful.

As shown above, the Tau Data Group's cuts were very efficient at eliminating the two photon and the wide angle Bhabha contaminates from the sample, but the cuts still left about a 1% contaminate from both muonic and hadronic events.

Purification Cuts on the Tau data Sample

Quantity	Restriction	Purpose
Highest momentum track in either hemisphere	Must be at least 168.5 degrees apart	Multihadron
	pass within 2 mm of the primary vertex	Cosmic Rays, Beam Background
	Contain at least 1 GeV	Multihadron
	$\|\cos\theta\| \geq 0.75$	Fiducial Volume
Sum on charge on hemisphere	+1 on one and -1 on opposing hemisphere	Multihadron
All charged tracks on one side of event	fall within a 20 degree cone about the maximum momentum track	Multihadron

Table 3.5

In order to improve the purity of the tau sample, make the forward backward determination unambiguous, and restrict the fiducial volume to the region for which the tracking efficiency is relatively flat, the further restrictions given in table 3.5 were imposed upon to the event sample which had already passed the tau groups cuts.[1]

Again, these cuts reflect the physics of the tau decay. As discussed earlier, the majority of tau decays have only one charged track, hence the energy requirement on the highest momentum track. In order to classify events, the highest momentum track of the event was used to define the axis of the hemispheres. This is shown in figure 3.3.

Hemisphere Division of a Tau Event

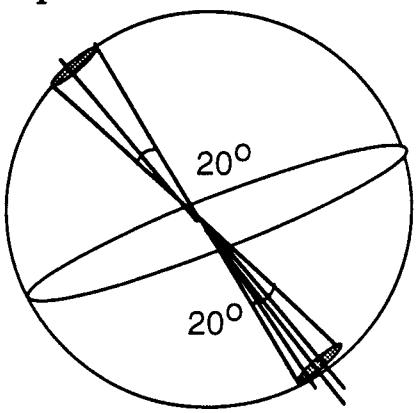

Figure 3.3

In order to further reduce contamination from multihadron events, all charged tracks on one hemisphere of the event were forced to fall within a 20 degree cone about the maximum momentum track on that hemisphere (also shown in figure 3.3). An additional cut was added to force the net charge on either hemisphere to be -1 on one side and +1 on the other so that the net charge on the tracks reflects the sign of their parent tau. The cut forcing the two highest momentum tracks to pass within 2 mm from the primary vertex was placed on the sample to prevent beam backgrounds such as SLC muons produced by beam scrapping, or cosmic rays passing through the detector from entering the sample. The fiducial volume cut

reflected the drift chamber's tracking inefficiencies and limitations in the region nearer than 45 degrees to the beam axis.

For Monte Carlo events passing the tau group's cuts, these additional cuts had the effects listed in table 3.6

Effects of Additional Purification Cuts

Type	Efficiency of Purification Cuts	Total Efficiency of Both Sets of Cuts	Expected Sample per Tau
Tau	0.702	0.4352	1.0
Hadronic	0.0025	5.1×10^{-6}	0.0004
Muons	0.45	0.0006	0.00144

Table 3.6

The total efficiency for taus was 43.5%. Two photon background were estimated near 0.3% level and the muon sample was cut to only 0.14%. The wide angle Bhabha backgrounds were less than 0.1%. Both the wide angle Bhabha and muon asymmetries were roughly equal to that of the tau. Thus, the contamination from background leptons should have little effect on the total measured asymmetries for taus and thus contributes only minutely to the total error of the measurement. The hadronic sample was cut to an insignificant level. So, systematic errors due to backgrounds are negligible in comparison to other sources.

By using the requirement that a event must pass within 2 mm of the primary vertex, it was estimated that less than one event due to cosmic radiation would enter the tau sample.

3.4 Tau Kinematic Effects

The effect of the cuts were examined in Monte Carlo to see their effects on the efficiency as a function of angle. The measurement of the electroweak asymmetry is acomplished by observing the production angle (θ) of the tau. So if the cuts produced a sample of data for which the efficiency depended on the angle of the maximum momentum particle, it would introduce an artificial bias into the measurement of the physical asymmetry. So in order to check for this effect, the net efficiency was plotted for both left and right handed Monte Carlo events. These plots may be seen in figure 3.4. These plots were made using MC tau events and passing them through the two sets of cuts. They give the net efficiency of both the tau group's cuts and the purification cut on the data sample as a function of cos(θ).

Net Efficiency using Both Sets of Cuts for Right and Left Handed Events

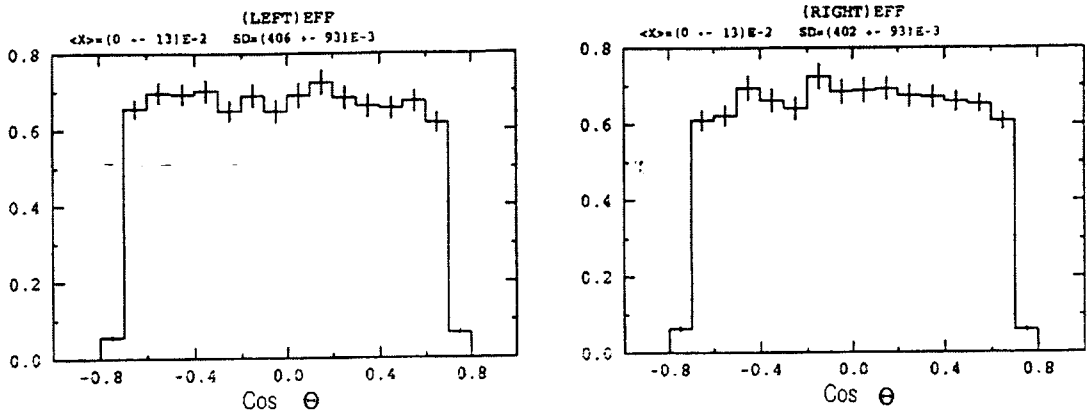

figure 3.4

Part of the reason that the efficiency plots need not be flat with respect to cosine of the production angle is that the decay kinematics of the tau depend upon its polarization state. The decay kinematics combine with the effects of the purity cuts on the energy of the maximum momentum track to give an efficiency which depends on angle. So as stated earlier, the slight cos(θ) dependence of the efficiency of the purification cuts tend to bias the measured value of A_τ away from the value predicted by the standard electroweak theory.

In the tau decay there is a correlation between the net polarization of the tau and the direction and energy of maximum momentum charged track. (This effect has been titled the V-A effect.) Since the Z^0 is polarized along the beam axis, there must be some correlation between the helicities of the final state tau pair. So when the taus decay, their decay products must also reflect the Z^0's spin state.

First, take the example of the decay mode: $\tau^- \rightarrow e^- \overline{\nu}_e \nu_\tau$. The best way to understand the spin-direction correlation in the tau rest frame is with a diagram as shown in figure 3.5.[3] This figure examines the case when the electron has the maximum momentum in the tau's rest frame compared to all the other tau decay products. In order for this to be true, the two neutrinos must be emitted in the direction opposite to the electron. The ν_τ always has a positive helicity state and the $\overline{\upsilon}_e$ always has a negative helicity state, so the sum of the z components of the total angular momentum due to the two neutrinos is zero. Since the net z component of the angular momentum due to the two neutrinos is zero, the z component of the spin of

the electron must reflect the initial z component of spin of the tau But it must also conserve total angular momentum and have the opposing helicity to the $\overline{\upsilon}_e$, if it is examined in the massless electron limit.[4]

Decay Correlations of $\tau \to e\nu_e\nu_\tau$ for Electron having Maximum Momentum

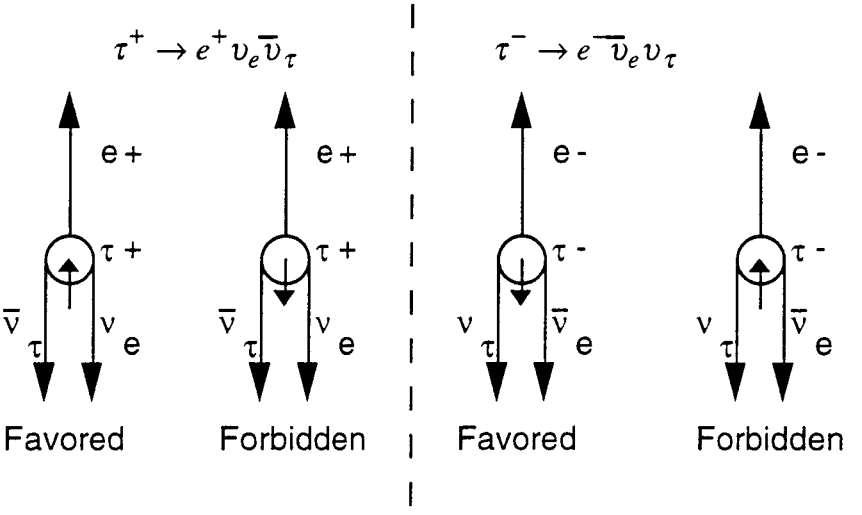

Figure 3.5

Therefore, examining the decay in the tau's rest frame, the electron has maximum energy if it is emitted opposite to the direction of spin of the tau. Exactly the opposite is true for $\tau^+ \to e^+ \upsilon_e \overline{\upsilon}_\tau$ because of the opposite helicity of the ν_e; the positron will have maximum energy if it is emitted in the same direction as the direction of spin of the tau. So, there is a correlation between the direction of polarization of the final state tau and the daughter electron's momentum direction. A similar argument may be made for the modes - $\tau^- \to \mu^- \overline{\nu}_\mu \nu_\tau$ and $\tau^+ \to \mu^+ \upsilon_\mu \overline{\upsilon}_\tau$; that is that the outgoing μ^+ will

tend to travel in the same direction as the spin of the tau; and the outgoing μ^- will tend to travel in the opposite direction as the spin of the tau.

A second decay mode of the tau that also shows this same bias is $\tau^- \rightarrow \upsilon_\tau \pi^-$ or $\tau^+ \rightarrow \bar{\upsilon}_\tau \pi^+$. The spin dependence of this mode is (perhaps) a bit easier to understand. The pion is a scalar particle, hence all the spin information in the decay must be transmited by the outgoing neutrino. Other decay modes of the tau show similar tendencies in prejudicing the direction of the outgoing particles.

The main lab frame consequence of the above effects are that the energy of the maximum momentum track is correlated to the production angle. There are specific cuts which target the energy of the maximum momentum charged track. So this bias in the energy distribution produces a slight cos(θ) dependance to the net effeciency.

Also related to the kinematics of the tau decay is the angle between the tau track and the angle of the maximum momentum particle which was used to identify it. By using Monte Carlo events, both the angle of the maximum momentum track and the tau's angle itself could be found. Histograms of $\{\mathrm{Cos}(\theta_\tau) - \mathrm{Cos}(\theta_{max})\}$ were made for all left and right handed events (shown in figure 3.6) . It was found that a gaussian could be fit to each histogram.

Gaussian Fit for

$Cos(\theta_\tau)$ - $Cos(\theta_{max})$

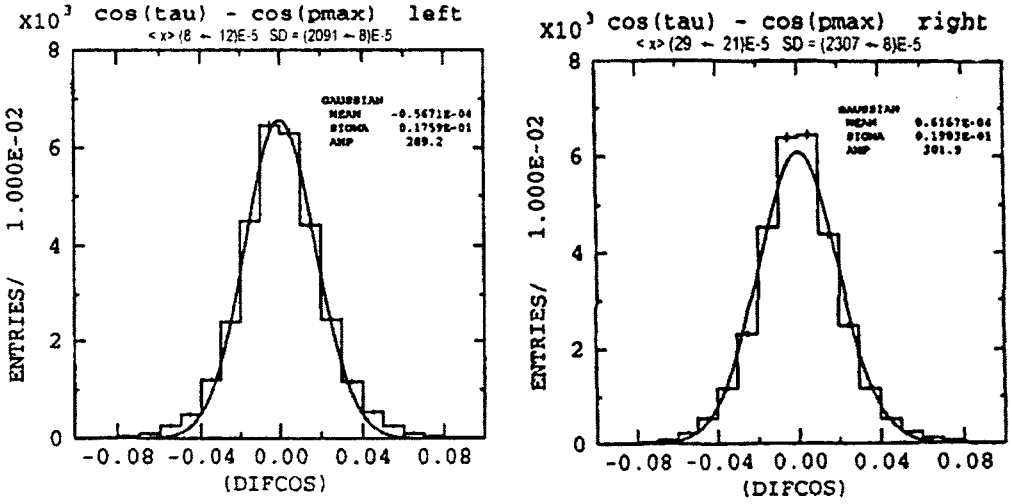

Figure 3.6

The gaussian fit to the plot of $Cos(\theta_{tau})$-$Cos(\theta_{max})$ described above was performed for four ranges of angles separately for both left and right handed events. (figure 3.7) Both the width and the mean of this distribution show some $cos(\theta)$ dependence. There is a small difference between the width of the gaussian between small and large angles but has a negligible effect on the measured asymmetry. Also there was a slight change in the mean of the gaussian for higher angle tracks but again this shift in the mean produced a very slight shift in the asymmetry which could be neglected to first order. So, both of these effects have a small effect on the measured value for A_τ but it assumed to be accounted for in the Monte Carlo correction to A_τ.

Sigma and Mean for

$Cos(\theta_{tau})$-$Cos(\theta_{max})$

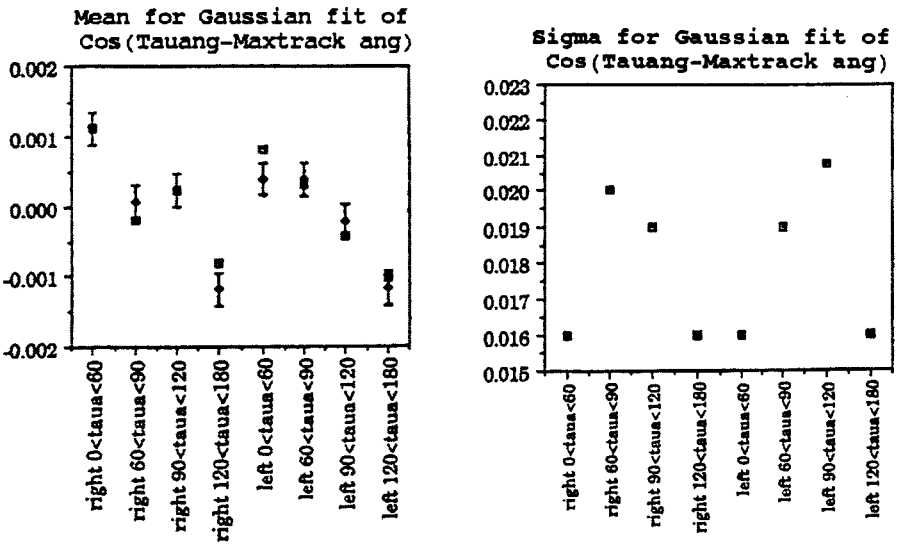

Figure 3.7

This bias has been studied with Koral Z Monte Carlo by comparing the value of A_τ calculated from exact momentum and charge information in all τ pairs produced by the Monte Carlo and comparing to the value after the same events have been decayed, reconstructed, cut and analyzed as real data. This difference between these two sets of data was found for two different methods of determining A_τ. So a correction factor was found for both methods that were used to determine A_τ. The details and size of these corrections will be given in the two analysis sections in chapter 4.

- 3.5 Wrong Hemisphere Assignment

In about 0.1% of the events, the wrong forward-backward assignment is made because the event produced a tau pair at close to 90^{o} to the beampipe and the maximum momentum track was found in the opposing hemisphere or in very rare cases the charge of each side was misidentified. This effect is assumed to be accounted for in the Monte Carlo correction discussed in section 3-4.

- 3.6 Polarization Measurement Errors

There were also errors in the Compton polarimeter's measurement of the polarization of the electron beam. There was a 1.3% error[5] in the beam polarization measurement for the 1993 data sample and a 0.63% error[6] in the polarization measurement for the 1994-95 data sample. Both of these errors were accounted for by adjusting the measured polarization accordingly.

In addition, there was a second error which is more subtle which contributed to the error in the polarization measurement. This factor was named the Chromaticity Effect. The error was introduced because the Compton polarimeter measured the polarization of all electrons including those which were not at the core of the beam. By examining the beam profile, it can be shown that there is a substantial low energy tail outside the core of the beam that has a lower polarization than the rest of the beam. The luminosity, however, comes dominantly from the core of the beam, so

the measured Compton value is lower that a proper luminosity weighted value. In other words, the Chromaticity effect has the effect of moving the polarization measurement to a lower value. The Chromaticity effect was measured to be 1.7%[6] for the 1993 run and 0.2% for the 1994-95 data run.[7] This effect was accounted for by adjusting it by a factor of 1.02 to the measured asymmetry for the 1993 run and 1.002 for the 1994-95 sample.

3.7 Radiative Corrections and Interference Terms

Radiative Corrections to the Measured Cross Section

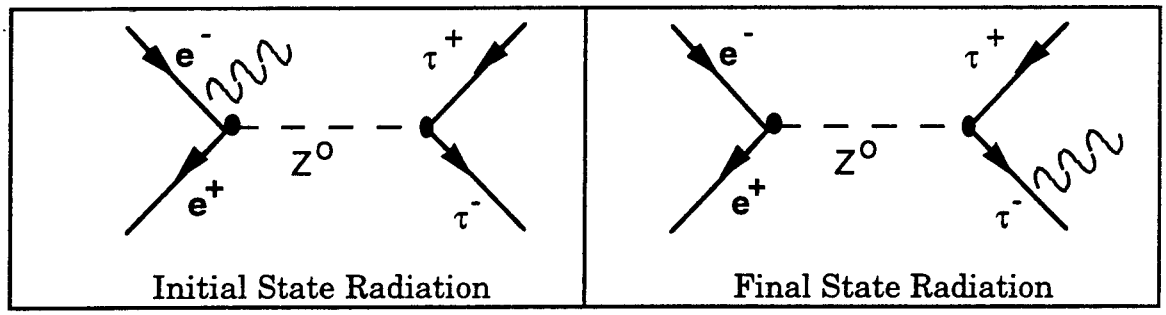

figure 3.8

The cross section which is used to define the parameter A_τ, that was given in chapter 1, is only a tree level calculation and thus does not take into account radiative corrections (as shown in figure 3.7) or γ-Z and γ-γ interference terms. The effect of these corrections for the muon have been determined in the Zfitter program by M. Swartz.[8] It was assumed in this analysis that these corrections although calculated for the muon were nearly correct for the tau. He calculated a correction of -0.004 for the

method and a correction of -0.005 for a log likelihood measurement due to the γ-Z and γ–γ exchange terms and radiative corrections.

A summary of the backgrounds and systematic errors which have been discussed in this chapter in the measurement and their respective magnitudes is contained in Chapter 4.

Chapter 4

Measurements of the Electroweak Asymmetry Parameter

4.1 Measurement using Left Right Improved Forward-Backward Asymmetry Technique

As stated in chapter 1, one method of calculating the electroweak asymmetry is by calculating the left-right improved forward-backward asymmetry. The events which passed though both the tau group's set of cuts and the additional set of purification cuts were then divided into forward and backward events with polarization left or right. The left-right improved forward-backward asymmetry was defined as

$$\tilde{A}_{fb} = \frac{(\sigma_{LF} - \sigma_{LB}) - (\sigma_{RF} - \sigma_{RB})}{\sigma_{LF} + \sigma_{LB} + \sigma_{RF} + \sigma_{RB}}. \qquad (1.10)$$

If the luminosity of the beam is assumed to be the same for both left and right polarizations and the degree of polarization of the electron beam is constant, then the definition given for $\tilde{A}_{fb}$ for the left right improved forward-backward asymmetry may be redefined. The cross section (σ) may be replaced by number ($N=\sigma L$) since the luminosity is equal for both polarizations. By using this division of the event sample, $\tilde{A}_{fb}$ was calculated as

$$\tilde{A}_{fb} = \frac{(N_{LF} - N_{LB}) - (N_{RF} - N_{RB})}{N_{LF} + N_{LB} + N_{RF} + N_{RB}}. \qquad (4.1)$$

Both 1993 and 1994-95 events in the SLD tau data sample were divided into forward, and backward events for left, and right polarizations.

Categorization of Events

	1993	1994-1995
N_{rf}	124	324
N_{rb}	171	426
N_{lf}	167	492
N_{lb}	162	451

Table 4.1

Table 4.1 lists the number of events which fall into each of the respective categories.

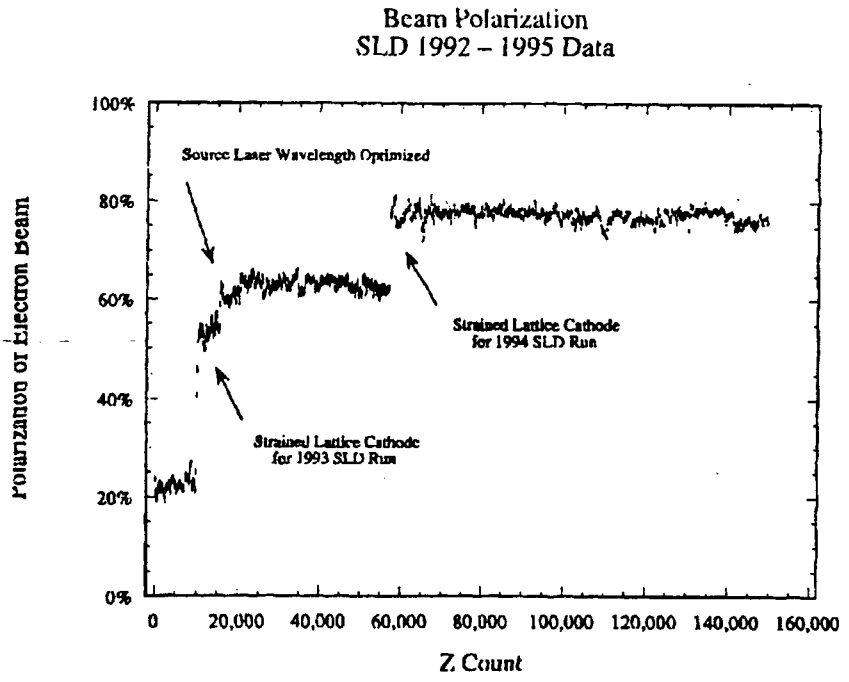

Figure 4.1

A major disadvantage of using $\tilde{A}_{fb}$ the method of calculating the asymmetry is the requirement that the polarization is constant for the period which each $\tilde{A}_{fb}$ calculation is made. During both the 1993 and the 1994-95 run the polarization ramped up from a low initial value. This is shown in figure 4.1.

Because of this requirement of constant polarization, restrictions were placed on the net polarization of the events that were counted to measure $\tilde{A}_{fb}$. These were that for 1993 data the net polarization of the beam had to be greater than 62% and for 1994-95 data the degree of polarization was forced to be greater than 76%.

As discussed in chapter 1, the forward-backward improved left-right asymmetry is related to the electroweak asymmetry by

$$\tilde{A}_{fb} = \frac{3}{4} P A_{\tau}. \tag{1.10}$$

However, this is only true if the detector was fully hermetic. As discussed earlier, the detector tracking becomes inefficient in the region closer than 45 degrees to the beam pipe. Therefore, the value of 3/4 must be corrected by a factor which takes into account this inefficiency of the current tracking routines used in reconstruction of events. So the relationship between the left-right improved forward-backward asymmetry and the electroweak asymmetry is changed to

$$\tilde{A}_{fb} = kPA_{\tau}. \tag{4.2}$$

where k is defined as

$$k = \frac{2\int_0^{0.7}(x)dx}{\int_0^{0.7}(1+x^2)dx} = 0.6017 \qquad (4.3)$$

where x=cos(θ). The limits on the integrals represent a hard fiducial volume cut at 45 degrees. Note that if the limits were increased to include the entire volume of SLD, then $k = \frac{3}{4}$ as expected. In order to obtain a better estimate for k, the Monte Carlo taus which passed the purity cuts were plotted as a function of Cos(θ) and then divided by the total Monte Carlo sample as a function of Cos(θ) to form an efficiency plot. This is shown in figure 4.2.

Fitting Function to Angular Efficiency

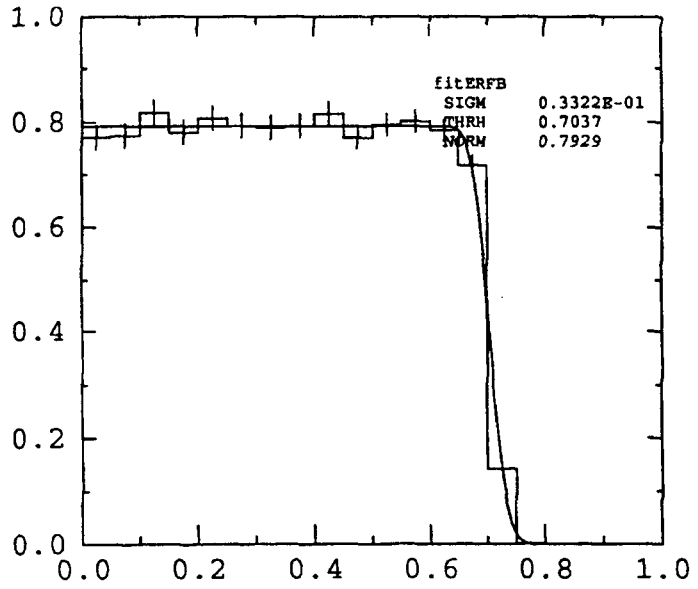

Figure 4.2

MINUIT (a least square fitting algorithm from the CERN library) was used to fit a functional form to the plot. The plot was fit to the following function.

$$\varepsilon(x) = Norm\left(\frac{1}{2} - \frac{1}{2}erf\left(\frac{|x| - thrsh}{\sigma}\right)\right) \tag{4.4}$$

where $erf = \frac{2}{\sqrt{\pi}}\int_0^1 e^{-u^2}du$ and x=Cos(θ). Thus, the correction factor could now be written as

$$k = \frac{2\int_0^1 \varepsilon(x)(x)dx}{\int_0^1 \varepsilon(x)\left(1+x^2\right)dx} \tag{4.5}$$

MINUIT fit the function to the efficiency plot and found the following values for all three of the parameters in Erf(x,σ,thrsh):

$$\sigma = 0.0332 \pm 0.00024$$

$$\text{thrsh} = 0.7037 \pm 0.0056$$

By inserting these values into the Erf function and then numerically integrating of equation 4.5, the value of k was determined to be

$$\text{k} = 0.604 \pm 0.013$$

With the measurement of this correction factor (k) and the net polarization for the run, the measured forward-backward improved left-

right asymmetry could be converted into a measurement of the electroweak asymmetry for the tau lepton. The final results are given in table 4.2.

The measurement error was dominated by low statistics. The variance of the asymmetry as a function of the number of taus was calculated to be

$$\mathrm{Var} = \frac{0.964}{n_{Tau}} \quad \text{or} \quad \sigma_{STAT} \approx \frac{1}{\sqrt{n_{Tau}}}. \tag{4.6}$$

Year	Number of Taus	Polarization	Asymmetry
1993	624	0.633	0.219± 0.105
1994 - 95	1693	0.775	0.181 ± 0.052

Table 4.2

The 1993 value has been corrected for the chromaticity effect. (An additional uncertainty of 0.0045 has been added in quadrature for the 1993 data. This is due to the additional uncertainty in the polarization measurement due to chromaticity in the 1993 data not matched in the 1994-95 data.). The asymmetries for right and left handed events can be seen below in figure 4.3.

The two sets of runs are combined according to their statistical errors as:

$$A_{\tau(Total)} = \frac{\dfrac{A_{\tau(1994-95)}}{(\sigma_{1994-95})^2} + \dfrac{A_{\tau(1993)}}{(\sigma_{1993})^2}}{\dfrac{1}{(\sigma_{1994-95})^2} + \dfrac{1}{(\sigma_{1993})^2}} \qquad \sigma_{total} = \sqrt{\frac{1}{\dfrac{1}{(\sigma_{1994-95})^2} + \dfrac{1}{(\sigma_{1993})^2}}} \tag{4.7-8}$$

where A_τ is the asymmetry for that given year and σ is the statistical error for that year.

Angular Distribution for Right and Left Handed 1993 and 1994-95 Tau Events

1993

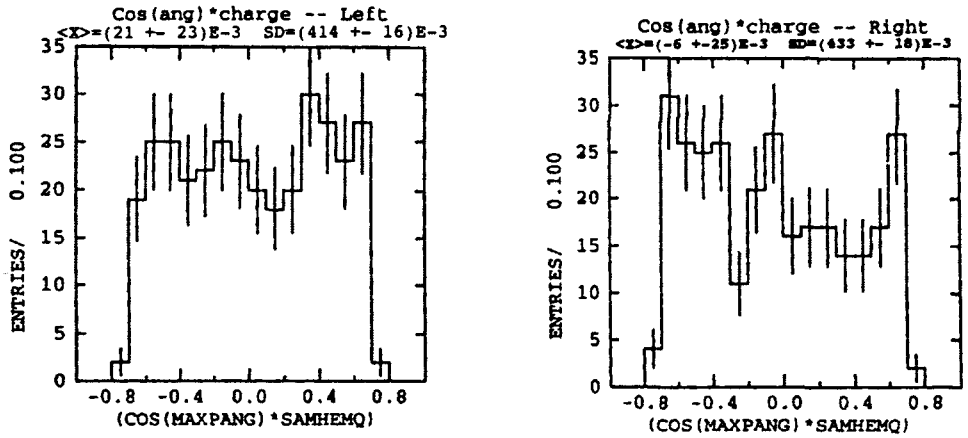

1994-95

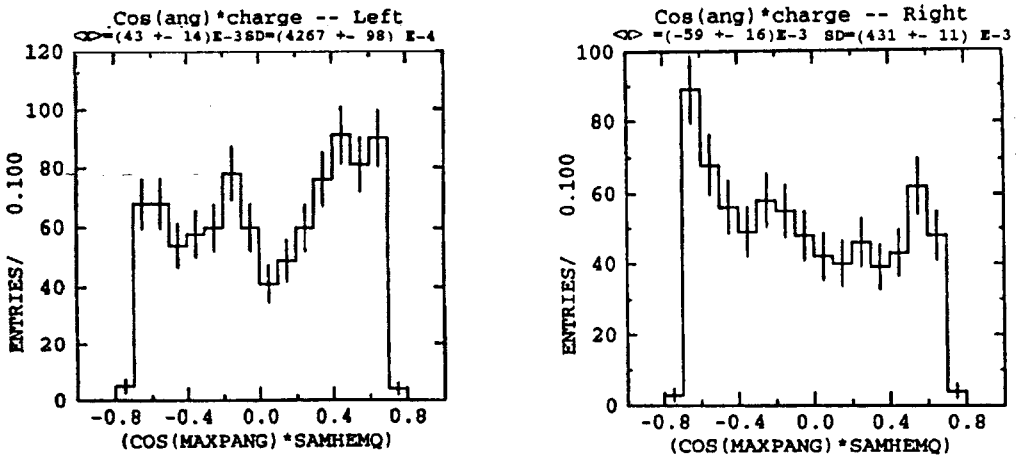

Figure 4.3

$\tilde{A}_{FB}$ Method

Backgrounds

Two Photon Events	Less than 0.1 %
Wide Angle Bhabhas	Less than 0.1%
Muons	0.14%
Hadron	0.02 %
Cosmic ray flux	Nil
Misidentified Hemisphere	0.1%

Corrections
(all relative)

Chromaticity Effect	1.7±1.1% 0.2± .05%	(1993) (1994-95)
Interference Terms γ-γ term γ - Z Term (off peak running) Radiative Corrections	-0.004	
Monte Carlo correction (V-A effect, Misidentified Hemisphere, etc.)	-0.0125	

Significant Systematic Uncertainties
(all relative)

Error in k	1.3%	
Error in beam polarization measurement	1.1%	(1993)
	0.05	(1994-95)
Limited Monte Carlo Statistics	2.5%	

Table 4.3

Two corrections were made to this measurement. First, a Monte Carlo correction was made which accounted for the V-A effect, misidentified hemispheres, etc. as discussed in section 3.4. This correction was made by comparing the calculated of $\tilde{A}_{fb}$ for raw generator level tau information and the value of $\tilde{A}_{fb}$ for taus which have been have been decayed, reconstructed, cut and analyzed as real data. The difference between these two sets was found to be 0.0125 ± 0.01. Second, the correction for

interference term and radiative corrections discussed in section 3.5 was applied. The tau electroweak asymmetry parameter was measured to be:

$$A_\tau = 0.175 \pm 0.046\ (\text{stat}) \pm 0.005\ (\text{sys})$$

4.2 Measurement using Log Likelihood Technique

The second method used to measure the electroweak asymmetry for the tau was the Maximum Likelihood Method. The data sample that was used consisted of the same 1993 and 1994-95 tau events which were used in the $\tilde{A}_{fb}$ analysis except that there was no limitation on the net polarization. The log likelihood method is a standard analysis technique that is described in many physics statistical analysis texts such as Lyones[1] and Eadie[2]. However a brief description will follow below.

The likelihood function is defined as a product of probability densities which are given as some function $f(x_i,\alpha_j)$. In this function, the variables x_i are measured quantities and α_j is some unknown parameter(s). The likelihood function is shown in 4.9.

$$L = \prod f(x_i, \alpha_i) \tag{4.9}$$

This likelihood function is calculated for a various values for the unknown parameter α. Thus, a value for α may be found which maximizes the likelihood function. To determine the most probable value of α, one usually

instead maximizes the function in terms of the log[f(x_i,α)] as in equation 4.10.

$$w = \log[L] = \sum \log\left[f(x_i, \alpha_i)\right] \tag{4.10}$$

Which has a maximum at a value of α such that:

$$\frac{dw}{d\alpha} = \frac{d}{d\alpha}\log[L] = \sum \frac{1}{f(x_i,\alpha)} \frac{df(x_i,\alpha)}{d\alpha} = 0 \tag{4.11}$$

The definition of one standard deviation is taken as the interval over which where the log[L] drops by 0.5* from its maximum value. In this case of this analysis, the probability density is proportional to the cross section for a $e^+e^-_{L,R} \rightarrow Z^O \rightarrow \tau^+\tau^-$ event. This cross section was given in equation 1-7. Thus, the likelihood function becomes the sum of the production cross section of every event measured in the tau data sample.

$$\frac{d\sigma}{d(\cos(\theta))} \propto (1 + PA_e\delta_{LR})(1 + \cos^2(\theta)) + 2(P\delta_{LR} + A_e)A_\tau \cos(\theta) \tag{1-7}$$

Remember in the definition of the cross section, that δ_{lr} is +1 for a left handed beam and -1 for a right handed beam, P is the magnitude of the polarization of the beam and A_l is the asymmetry of the electron and the tau respectively. Thus the log likelihood function is defined as

* NOTE: not 50% of the maximum value, but where the function drops by a value of 0.5

$$w = \sum \mathrm{Log}\left[f\left(P_i, \cos(\theta_i); A_\tau\right)\right] = \sum_{\substack{\text{All} \\ \text{Events}}} \mathrm{Log}\left[\frac{d\sigma}{d(\cos(\theta))}\right] \qquad (4.12)$$

So for this analysis, the variables (x_i) in the formulation of the log-likelihood are the angle of the maximum negative charged track given as θ (which is an approximation to the angle of the tau, since the tau cannot be observed directly) and the polarization of the beam. A_τ is the parameter α, which is varied over a fixed range so that it may be maximized. Thus, for clarity the log-likely function $f(\{x_i\},\alpha_i)$ may be rewritten as $f(\{\theta_i,P_i\},A_\tau)$ (as shown in eqn 4-12). A_e is fixed to its standard value 0.155[3] as measured by CERN and SLD. In order to reflect vertex corrections due to initial and final state radiation, the observed value of A_e might vary from this Born level value because of these higher level corrections. It was found, however, that the measured value of A_τ using the log likelihood method was insensitive to this small variation of A_e.

In order to determine the V-A effect on the measured value for A_τ, the value for A_τ was determined at two different stages of running Monte Carlo data. These stages were generator level events, and events passing all cuts, just as it was done for the method $\tilde{A}_{fb}$. So the net effect of the cuts and using the maximum momentum track on the MC tau data sample appears to be that the measured asymmetry using the maximum momentum track (as one must for a real tau since the tau decays at virtually the interaction point) seems to be 0.010 higher than the raw asymmetry of the generator level taus as measured before any restrictions were placed on them. This is if about the same size as with the Monte Carlo correction of 0.0125 observed

using the $\tilde{A}_{fb}$ method described in section 4.1. Thus, from this analysis one may conclude that the asymmetry that is measured on real data is 0.01 too high because of the V-A effect, and other effects discussed in section 3.4 and thus must be corrected for.

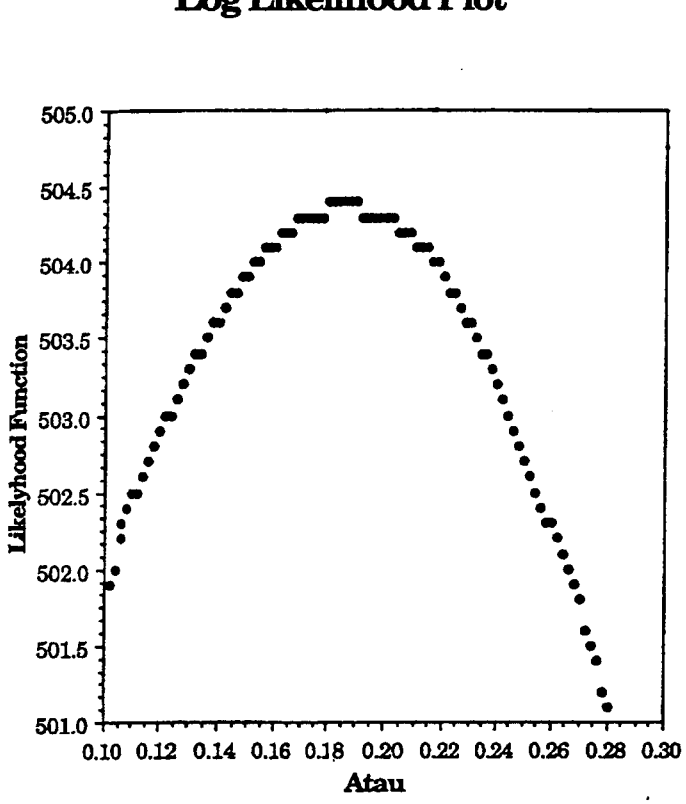

Figure 4.4

The real filtered tau data for the 1993 and 1994-95 runs were subjected to the same log likelihood analysis. (see figure 4.4) Note that unlike $\tilde{A}_{fb}$, all the data could be used and not only the data where the polarization is constant. So the event sample increased from 2730 events to 3155 events. The log likelihood method found that A_τ=0.193±0.05. Making the -0.010 Monte Carlo correction described above and the -0.005 correction for

radiative corrections and interference terms; the net asymmetry using the log likelihood method is

$$A_\tau = 0.179 \pm 0.040 \text{ (stat.)} \pm 0.0038 \text{ (sys.)}.$$

Likelihood Method

Backgrounds

Two Photon Events	Less than 0.1 %
Wide Angle Bhabhas	Less than 0.1%
Muons	0.14%
Hadron	0.02 %
Cosmic ray flux	Nil

Corrections
(all relative)

Chromaticity Effect	1.7±1.1% 0.2± .05%	(1993) (1994-95)
Interference Terms γ-γ term γ - Z Term (off peak running) Radiative Corrections	-0.005	
Monte Carlo Correction (V-A effect, etc.)	-0.010	

Significant Systematic Uncertainties
(all relative)

Error in beam polarization measurement	1.1% 0.05	(1993) (1994-95)
Limited Monte Carlo Statistics	2.5%	

Table 4.4

4.3 Comparison between Methods

With the $\tilde{A}_{fb}$ measurement which was only run on data from 1993 with polarization greater than 60% and 1994-95 with polarization greater than 75% we found that after all corrections were made to the asymmetry that

$$A_\tau = 0.175 \pm 0.046 \text{ (stat)} \pm 0.005 \text{ (sys)}.$$

With the log-likelihood measurement which was run on all events passing all sets of cuts regardless of the net polarization of the measurement of the asymmetry gave after all corrections that

$$A_\tau = 0.179 \pm 0.040 \text{ (stat.)} \pm 0.005 \text{ (sys.)}.$$

Note that there seems to be some difference between the two measurements techniques. However the two measurements were made using different samples. As a cross check, the log likelihood measurement was made with the same restrictions on the net polarization of the beam that was placed on the data for measurement via $\tilde{A}_{fb}$ (that is that the net polarization for 1993 events had to be greater than 0.63 and for 1994-95 events, it had to be greater than 0.75) When this restriction was placed upon the sample, the asymmetry was measured to be after all corrections

$$A_\tau = 0.173 \pm 0.041 \text{ (stat.)} \pm 0.005 \text{ (sys.)}.$$

Note that this measurement for the asymmetry is in good agreement with the value measured using the $\tilde{A}_{fb}$ method.

4.4 Conclusion

This analysis found that the electroweak asymmetry parameter for the tau lepton has a value of

$$A_\tau = 0.179 \pm 0.040 \text{ (stat.)} \pm 0.005 \text{ (sys.)}.$$

This is in good statistical agreement with the 1995 combined LEP[4] measurement for A_τ using data from all four experiments of

$$A_\tau = 0.142 \pm 0.008.$$

Also, The measurement discussed in this thesis seems to agree with the 1995 measurement by SLD of the electroweak asymmetry for the electron. SLD measured

$$A_e = 0.155 +- 0.004.$$

In conclusion, the measured value electroweak asymmetry for the tau using the SLD data sample seems to be in agreement with the measurement of the same asymmetry using the unpolarized electron beam made at the LEP experiments, and also the measurement of the asymmetry for the electron also made at SLD. So finally, it may be concluded that the

measurement of the asymmetry for the tau is in agreement with the assumption of lepton universality and thus is in agreement with the GWS standard model. It is expected that the SLD value for the electroweak asymmetry will improve with the increased statistics from the coming years' running.

List of References

Chapter 1

1 E. Fermi, *Z. Phys.* 161, (1934)

2 Mehra, Jadish, *The Beat of a Different Drum*, Oxford University Press (1994) p.457-459

3 C.S. Wu *et al.*, "Experimental Test of Parity Conservation" *Phys Rev*, 105, 1413 (1957)

4 R. Garwin, L. Leidermann and M. Weinrich, "Observation of the Failure of Conservation of Parity and Charge Conservation in Meson Decays: The Magnetic Moment of the free Muon." *Phys Rev*, 105, 1415 (1957)

5 J. I. Friedman and V.L. Telegdi, "Nuclear Emulsion Evidence for Parity Non-conservation in the decay chain π–μ-e." *Phys Rev*, 105, 1681 (1957)

6 Cheng, Ta-Pei and Li, Ling-Fong, *Gauge Theory of Elementary Particle Physics.*, Oxford University Press 1984, p.135

7 Mandel and Shaw, *Quantum Field Theory*, Wiley, 1993, p.239-242

8 Kaku, *Quantum Field Theory - A Modern Introduction*, Oxford University Press (1992) p.295-298

9 Pesken and Schroeder. *An Introduction to Quantum Field Theory.*, Addison-Wesly (1995) p. 294-700

10 Mandel, p 272

Chaper 2

1 Breidenbach, Martin. "SLC and SLD - Experimental Experience with a Linear Collider." SLAC PUB 6313

2 Partcle Data Book

3 Elia, Robert D. *Measurement of the Left-Right Asymmetry in Z Boson Production by Electron-Positron Collisions..* Ph.D. Thesis, SLAC Report - 429

4 Woods, M. *Polarization at the SLC* , SLAC Pub 6694 (1995)

5 Williams, David, *The Left-Right Forward-Backward Asymmetry for B Quarks at SLD*, Ph.D. Thesis, SLAC Pub 445 p.44

6 Ben-David, Ram Jacob. *The First Measurment of the Left-Right Cross Section Asymmetry in Z^o Boson Production*, Ph.D. Thesis, SLAC Report 442 p. 55

7 Elia, Robert, p. 51

8 CDC Design report p.5-27

9 Fero, et al. Performance of the SLD central drift chamber. Nuclear Instruments and Methods A:367 (1995) 111-114

10 SLD Design report ch 6

11 Fabjan, *Calorimetery in High Energy Physics* p359-360 from Ferbel's *Experimetal Techniques in High Energy Physics*

12 Ibid. p374-378

13 Axen et. al. *The Pb-Ar sampling calorimeter of the SLD detector* NIM A:328, p. 472-494

14 SLD design report 1-13

15 Ibid. p. 4-16

16 Ibid, p. 1-9

17 Williams, p. 65

18 Elia, p. 58

19 Ibid., p. 59-60

20 Ben-David, p.66-68.

21 Breidenbach, M

22 Fero, M *The Compton Polarimeter for SLC* (1992) SLAC-PUB-6026

23 Ibid

24 Blaylock, Guy *The WISRD Beam Energy Measurement* p. 1-2

25 Bambde et. al *Precision Measurements of the SLC Beam Energy*

26 Blaylock

Chapter 3

1 Ben-David, p. 71

2 Chan, Robert N. $e^+ e^-$ *Annihilation: New Quarks and Leptons* , Benjamin/Comming Publishing Company, (1985) p.379

3 Abe et al. "Measurement of the tau lifetime at SLD". *Phys Rev D.* Vol 52 No 9 Nov 1, 1995

4 Tsai, Youg-Su; "Decay Correlations of Heavy Leptons in $e^+e^- \rightarrow l^+l^{-*}$". *Phys Rev D.* Vol 4 No 9 Nov 1, 1971

5 Abe et al. "Precise Measurement of the Left-Right Asymmetry in Z Boson Production by e+ e- Collisions". PRL Vol 74 Number 1. 4 July 1994.

6 SLD Note To be published Eric Torrence

7 Schumm et al. "Estimate of the 1993 Chromatisity Effect on the 1993 Beam Polarization". SLD Note 240.

8 Swartz, Morris. "Radiative Corrections to Electroweak Measurements". SLD Physics Note 48.

Chaper 4

1 Lyons, Lewis *Statistics for Nuclear and Particle Physicists.* , Cambridge University Press (1986) p. 85-110.

2 Roe, Byron P. *Probrability and Statistics in Experimental Physics.* p. 118 130.

3 Pohl et al. *Physics of Tau Leptons.* CERN PPE/95-147 p.46

4 Ibid.

Biographical Sketch of Author

Brett Day Bolen was born on July 24, 1970 to Lee and Modine Bolen in Oxford, Mississippi. Both of his parents have taught at the University of Mississippi. Brett attended school in Oxford and graduated from Oxford High in 1989. He then enrolled at the University of Evansville in Evansville, Indiana. At Evansville, he was active in both the student congress and Amnesty International. He received his Bachelor of Science degree in Physics in May 1993.

After Brett's graduation from Evansville, he returned to Oxford to attend the University of Mississippi for his Masters of Science. During his first year, he began working for Dr. Robert Kroeger and the UM High Energy Group on analysis for the SLAC Large Detector (SLD). He went to Stanford for two summers to work at SLAC. Brett also taught labs at a variety of levels throughout his career at Mississippi.

Brett's extra-curricular interests include reading (he is a rabid science fiction fan), gaming, and Basketball. In high School he was a manager of the school basketball team for three years including one state championship team in 1987.

Mr. Bolen plans to continue his education in high energy physics. He will be attending Florida State University in the fall of 1996. He plains to obtain his Ph.D. from FSU and then begin work in both research and in physics education.